UNIVERSITA' DEGLI STUDI DI PADOVA

Facoltà di ingegneria

Dipartimento di Ingegneria meccanica settore Materiali

TESI DI LAUREA

Msc work carry out at the BME of Budapest Science and Engineering Material's Department and at the university of Padova Department of Engineering's Chemical Processing.

Effects of cold rolling on phase precipitation and phase transformation in a 2507 SDSS

Relatori: Prof. Calliari Irene

Dott. Mészáros István

Laureando: Bianchi Marco

ANNO ACCADEMICO 2010-2011

To my parents...

ABSTRACT

The aim of this work is to study the influence of cold rolling on the eventually $\gamma \rightarrow \alpha'$ transformation and in the phase precipitations, especially the eutectic decomposition $\delta \rightarrow \gamma_2 + \sigma$, after two thermal treatments.

In the present work 7 samples of UNS S32750 were cold rolled at different thicknesses, analyzed the percent reduction and after that, were quenched for 2400s at 400° and 900°C. The microstructures, after each treatment, were characterized by optical microscopy, scanning electron microscopy (equipped with EBSD), the chemical composition was confirmed with the EDS and the amount of ferromagnetic phases was determined with magnetic measurements with the AC Magnetization Curves tester, Forster magnetometer and Stäblein-Steinitz tester. It was found that in this type of Super Duplex Stainless Steel (SDSS) were not obtained enhancements for the magnetic properties, moreover, there was not transformation of phase ($\gamma \rightarrow \alpha'$) due to cold deformation. After the treatment at 900°C, a huge amount of sigma phase were precipitated in all the samples, but this phenomena was more accentued in the most deformed samples, hence, it is possible to say that the cold deformation improve the quantity of sigma phase that precipitate in the steel. In addition, it seems that at the decomposition process results, were obtained more secondary austenite than sigma phases, but that required further investigation.

This thesis was done in collaboration between the University of Padova, Department of Engineering's Chemical Processing, and the BME of Budapest, Science and Engineering Material's Department.

Summary

INTRODUCTION V

CHAPTER 1 1

The Duplex stainless steel

1.1 Duplex stainless steel 1

1.1.1 Influence of the elements 2

1.1.2 History 6

1.1.3 Main features 7

1.1.4 Uses and applications 8

1.2 The 2507 SDSS grade 9

1.3 The cold deformation 10

1.1.1 Phase transformations due to cold rolling 11

1.4 Secondary phases precipitation 14

1.4.1 The plastic deformation and its influence on the precipitation of σ phase. 17

CHAPTER 2 21

Sample preparation and OM and SEM analysis

2.1 Sample preparation 21

2.2.1 Etching 22

2.2 Analysis at OM 22

2.3 Electron scanning microscope 23

2.3.1 Back scattered electron 25

2.3.2 EDS 26

2.3.3 EBSD 27
2.4 Hardness 32
2.5 X-Ray diffraction 33

CHAPTER 3 37

Magnetic Investigation

3.1 Magnetism and its different classifications 37
3.2 Ferromagnetic materials 39
3.2.1 Ferromagnetism and Hysteresis loop 41
3.2.2 Magnetic behavior of γ and α 42
3.3 Magnetic tests 44
3.4 Ferrite tester 46
3.5 AC magnetization curves test 47
3.6 Försters magnetometer 48
3.7 Stäblein Steinitz test 49

CHAPTER 4 53

Data analysis

4.1 Optical metallographies 53
4.1.1 Phase volume fraction 57
4.2 SEM analysis 58
4.2.1 EDS analysis 61
4.2.2 EBSD investigation 64
4.3 Micro-hardness test 68
4.4 Ferrite tester 69
4.5 AC magnetization curves test 70
4.6 Förster magnetometer 72

4.7 Stäblein Steinitz test 74
4.8 X Ray diffraction 76
4.9 Comparisons and correlation 77
4.2.2 Martensite trasformation and magnetic tests results. 77
4.9.2 Sigma and austenite analysis 80

Conclusions 84
References 86

INTRODUCTION

The European norm EN 10088 defines the stainless steels as ferrous alloys with more than 10.5% chromium content. Their main objective is to resist to the corrosive environment, their excellent resistance to corrosion is due to their passivity property in a sufficiently oxidizing environment (e.g. air), forming a special film of absorbed oxygen on surfaces. This film protects the material below from corrosion. It can be re-form when is damaged, but only if the environment is sufficiently oxygenated and if the oxygen comes in contact with the material. It is the chromium that makes the steel able to form this oxide layer, as mention in the norm it has to be content in the percentage more than 10.5%. Only above this quantity, chromium oxide can form on the steel surface in quite benign environments. However, higher Cr contents must be added in order to give to the steel a very higher resistance against pitting and general corrosion in more hostile environments.

The elements of the alloy and the thermal treatments, determine the microstructure dividing the stainless steel in four big families:

1. Austenitic, this category of steel maintain completely the austenitic phase until room temperature thanks to the high presence of gamma-former elements. They show a very good resistance to corrosion, and can be excellent in some special environments.

2. Ferritic, alpha phase is always stable in this steels, mechanical features cannot be enhanced by thermal treatment but only by cold deformation.

3. Martensitic, essentially they contain only chromium, and the characteristic can be enhanced by quenching, it is the strongest kind of stainless steel. They are also hardenable in heat treatment.

4. Duplex (DSS) they consist of mainly two phases: ferrite and austenite, in ca. 50-50%. This ratio of the phases is resulted by high alloying element content with low carbon content. Evidently they have biphasic structure and their characteristic of corrosion resistance are the best of all, in relation to the mechanical resistance only the martensitic are better, while toughness in DSS are better than ferritic but worse than austenitic.

There are also other categories like the Precipitation hardening and the martensitic-austenitic but are not the “main” categories. These types of stainless steels have different properties: an example it is the different magnetic behavior, because fully austenitic stainless steels are non-magnetic, while martensitic and ferritic stainless steels are ferromagnetic; and this is a property that will be contributed to build the work.

Unfortunately, these steels are prone to give wide precipitation of secondary phases if are not carefully cooled, and in the DSS this behavior is enhanced. Therefore, will be presented the analysis of the sigma phase, the secondary phase most well-known.

The topic of this work is about a type of Duplex steel, the quite employed 2507.

Many articles talk about that some DSS after cold deformation present a transformation that lead a percentage of γ phase to transform in α' martensite depending on the rate of cold working. This is important because it changes the characteristic of the steel and also was verified in other duplex steel in previous investigations. This behavior is particular about the 2507, however a complete investigation with a series of sensible magnetic test (that immediately detect any variation of ferromagnetic phase content) give us the answer.

The investigation continues with the application of two different thermal treatments, one recovery type that does not affect the microstructure, but surely give an effect on the point defect concentration. The second treatment was at higher temperature (900°C) in order to begin the decomposition of ferrite phase. This treatment was supplied in order to understand if there is some influences of the deformation rate

(concentration of defects, increase in internal energy etc.) on the precipitation of the sigma phase in the eutectic decomposition of the ferrite.

Therefore, very important conclusion can be drawn after the investigation with the magnetic tests. Also EBSD analysis was carried out in this work, that give useful phase maps, leading the search to interesting issues that could be a hint for further investigations.

This work was started at the University of Padova, department of Engineering's Chemical Processing but was carry out mainly at the BME university of Budapest, Department of Science and Engineering Materials.

CHAPTER 1

The duplex stainless steel

1.1 Duplex stainless steel

Duplex Stainless Steels (DSSs) have a biphasic structure of austenite (γ) and ferrite (δ), with a ferritic matrix in which the austenitic phase and other alloying elements (chromium, nickel, molybdenum, manganese, silica) are present. The differences between DSSs and other stainless steels are their weldability, which is better than ferritic stainless steels, and their resistance to stress corrosion cracking, that is higher than austenitic stainless steels. DSSs are also not affected by the intergranular corrosion.

They have a higher pitting and crevice corrosion resistance than ferritic stainless steels and a resistance in strong acid environment similar to austenitic steels but the main advantages is their resistance to chloride stress corrosion cracking. The optimal temperature to use these steels is between 50÷250°C, because the toughness decreases too much below the minimum value, and the ferrite δ starts to be unstable above 250°C [1][2][12][6].

The pitting resistance of stainless steel it is primarily determined by their composition. The three main elements which have a significant beneficial effect are chromium, molybdenum, and nitrogen.

The formula that gives their respective contribution is:

PREN= %Cr + 3.3*%Mo + 16*%N.

PREN is Pitting Resistance Equivalent Number, and the percentages are in weight percent of elements in solid solution. This formula permit a first base classification based on the resistance against aggressive environments, but do not forget that is a macroscopic index, the microscopic locally variation of composition was not considered by the PREN. There is another index, the PREW, less used; it takes inconsideration also to the tungsten:

PREW: %Cr + 3.3 [%Mo + 0.5* %W] + 16* %N

However a high value of PRE means a high resistance to corrosion.
As known, ferritic stainless steels, cannot hold nitrogen in solid solution, must obtain all their corrosion resistance from chromium and molybdenum.
The nickel in austenitic stainless steel confers no direct benefit; it only stabilizes the austenitic structure, which can hold appreciable nitrogen.
In this way, it is possible to identify four different pitting resistance classes for Duplex Stainless Steels:
1) Lean DSS without Molybdenum (e.g. V2101Mn or 23Cr-4Ni-0.1N) that are good alternative to AISI 304 and AISI 316. (PREN≈25);
2) DSS like 22Cr-5Ni-3Mo-0.17N (PREN≈35);
3) DSS with 25% of Chromium, and with Molybdenum, Nitrogen, and sometimes Tungsten and Copper (PREN≈35÷40);
4) Super DSS like our 25Cr-7Ni-4Mo-0.27N and other similar but with a little bit of Tungsten and Copper (PREN≥40).
In the following table it is possible to see the difference between the classic 300 grades and the duplex family. Moreover is also shown the different composition of the steels and the different corrosion index results [4][7][9][11].

FAMILY	USA	EURONORM	Cr	Mo	Ni	Mn	Cu	N	Others	PRE	PREN	PRENW
300	304L	1.4307	18	0	9	1	0			18	18	18
	316L	1.4401	17	2	11	1	0			24	24	24
	904LN	1.4339	20	4	25	1	1,5	0,1		33	35	35
Standard DUPLEX (1996)	S 32304	1.4362	23	0	4	1		0,13		23	25	25
	S 32205	1.4462	22	3	6	1		0,17		32	35	35
	S 32750	1.4410	25	3,5	7	1		0,27		37	41	41
	S 32760	1.4501	25	3,8	7	1	0,7	0,27	0,7W	38	42	43
	S 32520	1.4507	25	3,5	7	1	1,5	0,25		37	41	41

Table 1: differences in composition and corrosion index between some widely used duplex and stainless steels [11]

1.1.1 Influence of the elements

The alloying elements have a specific effect on the properties of the steel. It is the combined effect of all the alloying elements and some extent, the impurities that determine the property profile of a certain steel grade. In order to understand why different grades have different compositions a

brief overview of the alloying elements and their effects on the structure and properties may be helpful. The effects of the alloying elements on some of the important materials properties will be discussed more detailed in the subsequent sections, especially the role of nitrogen on blocking the γ phase.

Chromium (Cr): this is the most important alloying element in stainless steels. This element gives to the stainless steels their basic corrosion resistance if is added more than 10.5%; as it is known chromium permit the steel passivity state. The corrosion resistance increases with increasing chromium content. It also increases the resistance to oxidation at high temperatures. Chromium promotes a ferritic structure; it stabilizes the alpha-phase reducing the domain of the gamma-phase.

Nickel (Ni): the main reason for the nickel addition is to promote an austenitic structure but also to increase the corrosion resistance. Nickel generally increases ductility and toughness. It also reduces the corrosion rate and is also advantageous in acid environments. In precipitation hardening steels nickel is also used to form the intermetallic compounds, which are used to increase the strength. It is a gamma former, and playing with the content of this element and the chromium it is possible to create a wide range of alloys.

Molybdenum (Mo): Molybdenum substantially increases the resistance to both; general and localized corrosion. It increases the mechanical strength, and strongly promotes a ferritic structure, which is why for obtaining duplex steel also the gamma-promoter has to be added. Molybdenum also promotes the formation secondary phases (sigma overall) in duplex steels but also in other kind of stainless steels. In martensitic steels it will increase the hardness at higher tempering temperatures due to the effect on the carbide precipitation.

Copper (Cu): Copper enhances the corrosion resistance in certain acids and promotes an austenitic structure. In precipitation hardening steels, copper is used to form the intermetallic compounds that increase the strength.

Manganese (Mn): Manganese is generally used in stainless steels in order to improve hot ductility. The effect on the ferrite/austenite balance varies with temperature: at low temperature manganese is an austenite stabilizer, but at high temperatures stabilizes only ferrite. Manganese increases the solubility of nitrogen and is used to obtain high nitrogen contents in austenitic steels.

Silicon (Si): Silicon increases the resistance to oxidation, although at high temperatures and in strongly oxidizing solutions at lower temperatures; promotes a ferritic structure.

Carbon (C): Carbon is a strong austenite former. It also substantially increases the mechanical strength. Carbon reduces the resistance to intergranular corrosion. In ferritic stainless steels carbon will strongly reduce, toughness and corrosion resistance. The duplex have a very low content of C, in order to permit the correct phase ratio, it can give rise with chromium to the chromium carbide that can precipitate after thermal treatment and reduce the neighborhood content of chromium, promoting the corrosion.

Nitrogen (N): Nitrogen is a very strong austenite former. It also substantially increases the mechanical strength. Nitrogen increases the resistance to localized corrosion, especially in combination with molybdenum. In ferritic stainless steels nitrogen will strongly reduce toughness and corrosion resistance. In the martensitic and martensitic-austenitic steels nitrogen increases hardness and strength, but reduces the toughness.

The effect of the alloying elements on the structure of stainless steels is summarized in the Schaeffler-Delong diagram (Figure 3). The diagram is based on the fact that the alloying elements can be divided into ferrite stabilizers and austenite-stabilizers. This means that they promote the formation of ferrite or austenite in the structure. If the austenite-stabilizers ability to promote the formation of austenite is related for nickel, and the ferrite-stabilizers likewise compared to chromium, it becomes possible to calculate the total ferrite and austenite stabilizing the effect of the alloying elements in the steel.

This gives the so-called chromium and nickel equivalents that are: Chromium equivalent = %Cr + 1.5 x %Si + %Mo; and Nickel equivalent =

%Ni + 30 x (%C + %N) + 0.5*(%Mn + %Cu + %Co). The next figure (fig 1) is the Schaeffler-Delong diagram that is used for the previous concept of Ni and Cr equivalent and show the displacement of the different grades of DSS and an approximation of the ferrite content in it.[5][4][7][9][10][11]

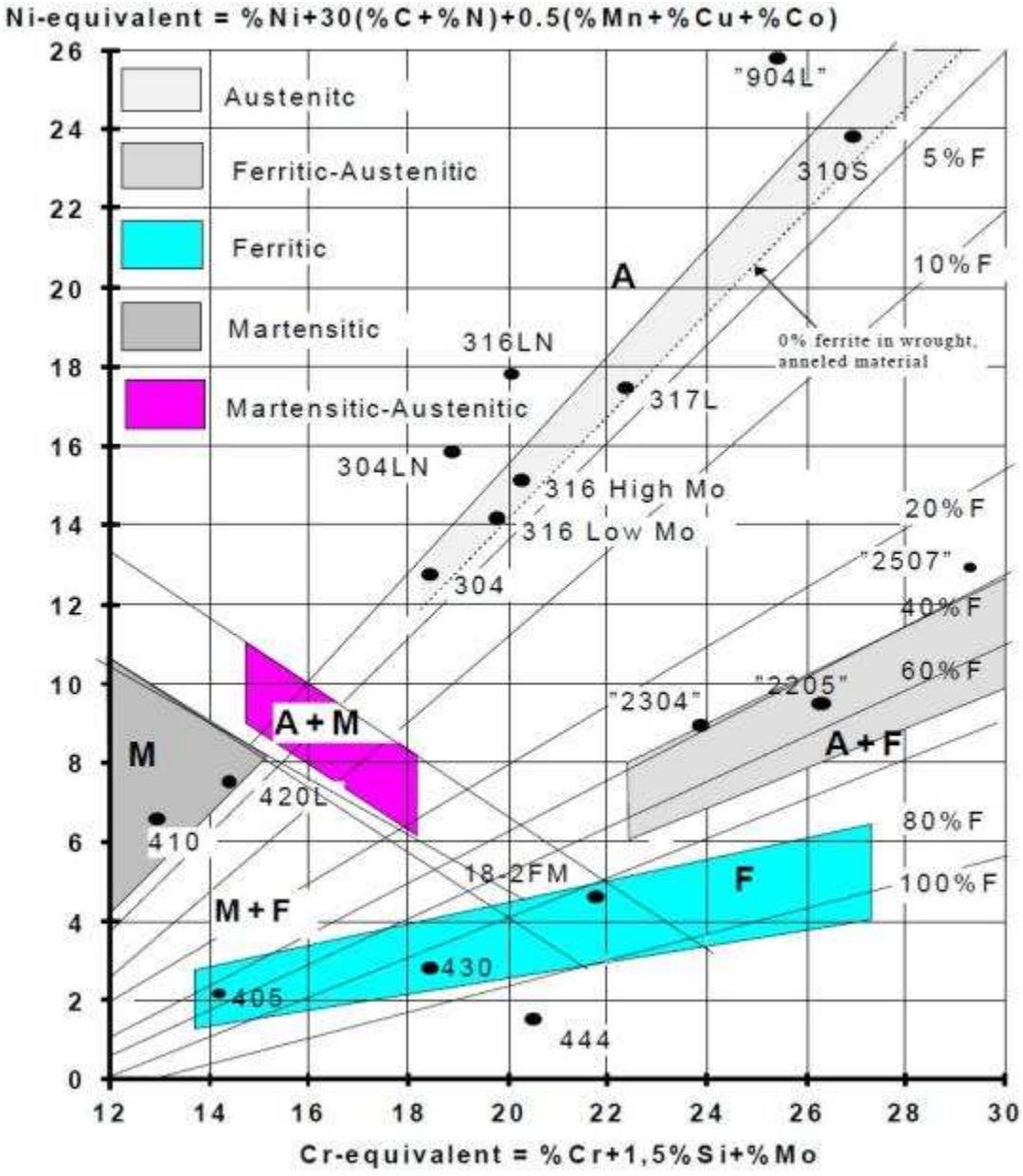

Figure 1: Schaeffler-Delong diagram with showed the percents of ferrite. There are also indicated some widespread stainlesssteels. [11]

1.1.2 History

The origin of the biphasic stainless steel dates back on the beginning 30's. In that years, in France and Scandinavian area, took place the first creation of some steels with austenite-ferrite matrix, for use in the sulfite paper industry. From the scientific point of view, the first mention for those steels can be found on the J.H.G. Monypenny's book: "Stainless Iron and Steel" about steels with biphasic structure; referring to a particularly microstructure with 50% ferrite - 50% austenite created following a Krupp patent for austenitic stainless steels pending on 1922.

The firsts industrial applications of these kinds of steel took place between 1930 and 1940, either on die cast and on hot worked. In that last kind of steel, it can be appreciate a sensible improvement of the

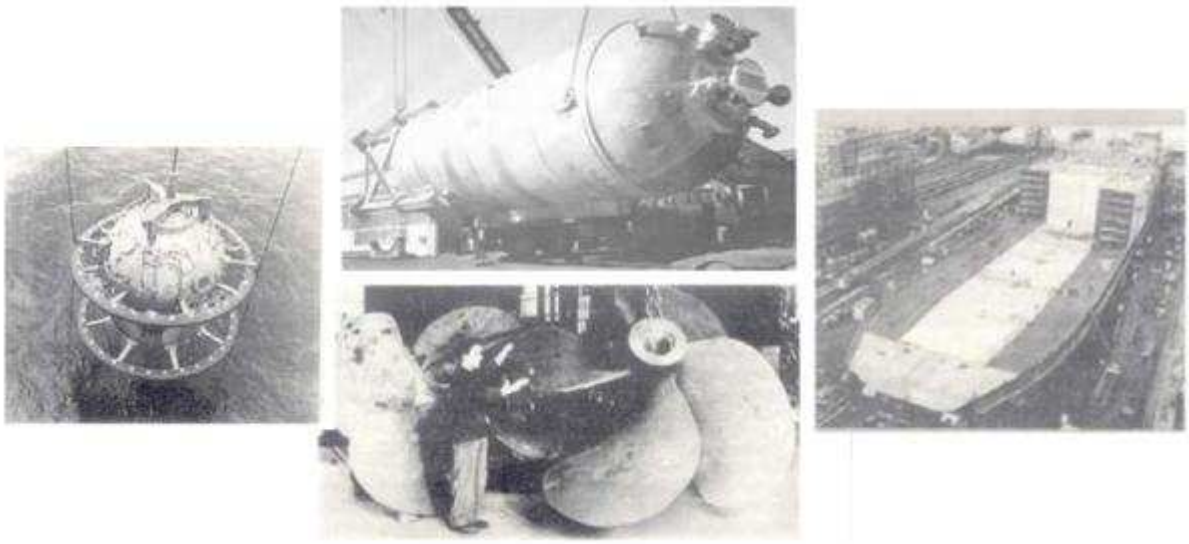

Figure 2 Typical application of the stainless steels in the 60es and the 70es.[9]

mechanical characteristic and the wear resistance.

Only on the 50's and the 60's the marketing of the semi finished stainless steel began. In those years the introduction of the American regulation AISI 329 (25 Cr / 5 Ni / 1, 5 Mo) took place, and in the same years also began the creation of the SANDVIK 3RE60 (18,5Cr / 5 Ni / 2,7 Mo), one of the forerunners of the modern double-phase stainless steels.

In the 70's the industries began to use new refining technology like AOD and VOD converter, thanks to this, the quality and all the mechanical features of stainless steels began to improve sensitively. In fact, the possibility to reduce the content of residual elements (such oxygen,

sulfur, carbon, etc.) and in the meaning give to the steel precise range of composition, particularly for the nitrogen content, improve to have sensibly for the corrosion resistance and the high temperature behavior of stainless biphasic steel. These manufacturing methods, together with the introduction of the continuous casting process, also allow a significant reduction in production costs.

In the end of the 70's were developed the chemical composition of a stainless biphasic steel with 22% of chromium and 5% of Nickel, there is also a small quantity of nitrogen, the steel was weldable, showed high mechanical resistance and was absolutely no prone to integranular corrosion.

Due to the versatility and the very good performances (although the composition was a little different between the producers) this steel knew a great diffusion among the end users. We are talking about the widespread and well known 2205 grade, the "workhorse" of the two-phase stainless steels. From 1980 the rapid diffusion of the biphasic stainless steels called *superduplex,* for application in particularly aggressive environments took place. The typical composition of these steels shows a 25% of chromium, a 7% of nickel and a 3% of molybdenum. A market disposition took in these years a developed class of biphasic stainless steels low-alloy, which the mainly is the SANDVIK 2304, which can be considered competitive to the traditional austenitic stainless steels AISI 304 and 316 in the environments where the resistance to stress corrosion cracking and the mechanical resistance are fundamental.[9][7][10]

1.1.3 Main features

The stainless steel was invented to improve the corrosion resistance in several environments. However, this steel was not so strong and stiff like the classics hardened steels, so, during the past years the duplex steels and the super duplex stainless steel has been developed to give, with high corrosion resistance also great mechanical features, sometimes more than the martensitic. Duplex stainless steel have about double the strength compared to austenitic stainless steels, contain only about half

the nickel concentration of typical austenitic stainless steels; they are also less expensive and sensitive to the price of nickel.
With the high chromium concentration, they have excellent chloride stress corrosion, improved resistance to localized corrosion, particularly pitting, crevice corrosion and stress corrosion cracking contain. The two phase mixture also reduces the risk of intergranular attack; for the same reason they are not prone to solidification cracking during welding. [41][9][5]

1.1.4 Uses and applications

Applications of ferritic-austenitic steels are typically those requiring high strength, good corrosion resistance and low susceptibility to stress corrosion cracking or combinations of these properties. The main uses of this kind of steels are on: brewery pipes and tanks, feedwater heater, flu gas scrubbers, oil and gas industries, tank trailers for hot chemicals, but this is not an exhaustive list.

Figure 3 Super duplex 2507 turbine feed pipeline. [35]

High alloyed grades, e.g. “2507”, are used in piping and process equipment for the offshore industry (oil and gas) and in equipment for environments containing high chloride concentrations, such as sea water. “2205 type” is for example used in pulp digesters and storage towers in the pulp and paper industry where it is rapidly becoming a standard grade. The 2507 grade it is also used in piping systems, heat exchangers, tanks and vessels for chloride-containing media in the chemical industry, in piping and process equipment for the oil and gas industry, in cargo tanks, ships for transport of chemicals, shafts, fans and other equipment which require resistance to corrosion fatigue. [9][46][39][5][35]

1.2 The 2507 SDSS grade

The SDSS belong to the family of the duplex steels. The term "Super-Duplex" was first used in the 1980's to denote highly alloyed, high-performance Duplex steel with a pitting resistance equivalent of >40 (based on Cr% + 3.3Mo% + 16N%). It means that is a high performance duplex based on a high chromium nickel and molybdenum content, this to enhance the pitting corrosion, while the presence of the nitrogen increase the structural hardening.

The UNS322750 (SAF 2507) is a duplex (γ-δ) stainless steel which is designed for demanding applications, which require exceptional strength and corrosion resistance such as chemical process, petrochemical and seawater equipment. The steel has excellent resistance to chloride stress corrosion cracking, high thermal conductivity, and a low coefficient of thermal expansion. The high content of chromium and molybdenum, helped by nickel copper and nitrogen, provide excellent resistance to pitting crevice and general corrosion. The impact strength is also high but it shows a badly prone to the hot working. The steel is not

recommended for applications which require long exposures to temperatures above 300°C because of the risk of a reduction in the toughness. All common methods including GTAW, SAW and GMAW can be successfully employed for welding. Targeted applications are equipment for the petrochemical industry, included the wide use of this steel on the off-shore equipment. Then other application fields are seawater piping for desalinization plants, scrubber system, heat exchangers in chemical industry.
The one used in this work, supplied by Avestapolarit in solution annealed condition, have the following composition. [4][5][9][46]

Element	**C**	**Si**	**Mn**	**P**	**S**	**Cr**	**Ni**	**Mo**	**Cu**	**N**
Quantity [%]	0.015	0.24	0.83	0.023	0.001	24.8	6.89	3.83	0.23	0.27

Table 2: Chemical composition of the steel under investigation

1.3 The cold deformation

In this work cold deformation is obtained by cold rolling. Is not so common to carry out the cold rolling in this kind of duplex, because of the hardness, is better to carry out a hot rolling, however in several cases the cold rolling is carry out for some applications like tubes, pipes etc.
The rolling consists of passing a piece of steel (beginning with a slab ingot or with a continuous casted piece) through two rolls separated by a distance less than the thickness of the beginning piece. The piece has to keep passing through such roll (or through the tandem rolling) until the final thickness is achieved, and as more reduction of thickness more will be the final length of the piece. A cold rolling gives to the piece an excellent tolerance on thickness and shape, indispensable with a strictly control on the final reduction, like in this work, is required. Unfortunately the cold rolling needs very high forces and these give rise to surface

stresses that can also be not uniform; this prevented us to carry out some tests. The high resistance of the material exposed to the deformation, caused the bending of the material, effect that can be canceled by multiple passages. Several methods can be used to decrease the force on the rolls: use of lubricants, carry out only small reduction per pass, use small diameter rolls etc.

The mechanical properties of stainless steels are strongly affected by cold work. In particular the work hardening of the austenitic steels causes considerable changes in properties after, e.g. cold forming operations. The general effect of cold work is to increase the yield and tensile strengths and at the same time decrease the elongation. It can be found a wide use of this technique on the austenitic stainless steel, less in the duplex and super duplex grades. [7][9][10]

1.1.1 Phase transformations due to cold rolling

Many studies have demonstrated that the FCC microstructure of most austenitic stainless steels is not thermodynamically stable around the room temperature.

Therefore, stress or plastic deformation may induce a less diffusion in martensitic phase transformation, by which the metastable austenite transforms to the thermodynamically more stable martensite α' type (ferromagnetic, that is different from the ε type, the thermal one that however, can be a step of the transformation). The presence of this austenite-martensite transformation may cause a multitude of problems, such as delayed cracking of deep-drawn austenitic stainless steel components.

Nevertheless, this transformation is important for the mechanical properties and may enhance the rate of work hardening but the main effects are the embrittlement of the steel.

The deformation induced transformation is classified in two types: the stress assisted transformation, where stresses help to start the transformation, even with the temperature above Ms (the quenching temperature of the steel). And the strain-induced martensitic transformation, where dislocations work as easier nucleation sites for the martensite. The stress-assisted transformation occurs at temperatures slightly above Ms, while the strain-induced transformation occurs at higher temperatures than Ms (e.g. room temperature) and is the case of the 2101 Lean DSS [7].

The strain-induced martensite forms by plastic deformation of the parent austenite, where the proper defect structure is created and acts as an embryo for the transformation product.

The result of the quenching of a steel in order to obtain martensite is, talking about free energy, the naturally formation of this new phase, that under a certain temperature begin to have lower free Gibbs energy respect to the former austenite, so it is energetically favored at Ms when it start the transformation. But, this transformation can take place also at temperatures above Ms, therefore when is not thermical favored. The statement is another kind of energy that reduces again the free G energy of the martensite reaching the enough energy gaps to start their formation. This other kind of energy is the stress energy induced in the material after a mechanical, plastic deformation. Moreover the amount of

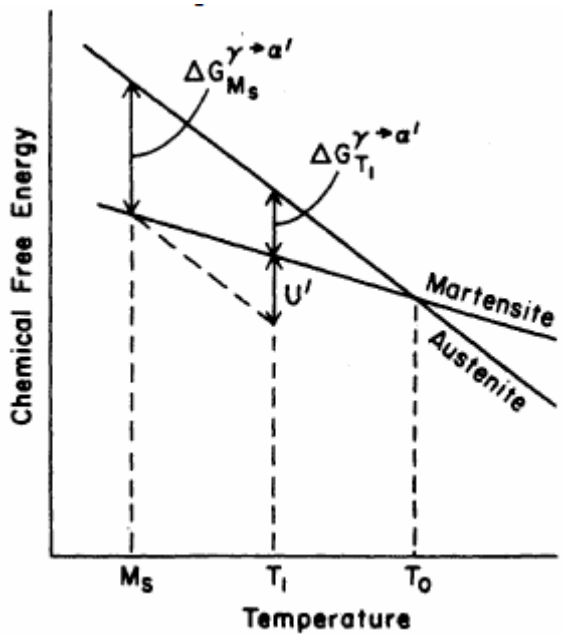

Figure 4: chemical free energies of austenite and martensite phases as a function of temperature

mechanical energy to supply the martensite transformation is dependant from temperature of working, composition and history of the material. It is possible to say that this supplied energy increase the temperature at which start the martensite transformation from Ms to Md, that is the temperature below which martensite will form under deformation.

Several authors studied this temperature Md giving formulas based on composition to predict the eventually formation of martensite in a steel.[22] The following formula of Md(30/50) indicate the temperature at which 50% of austenite transform to martensite under 30% of deformation:

Md (30/50)= 413- 13.7%Cr – 9.5%Ni – 8.1%Mn – 18.5%Mo – 9.2%Si – 462%(C+N).

A high value of Md (like the one showed in 301 and 304 grade steels) for a steel means that it is more susceptible to form martensite when is deformed at room temperature. Instead, steel with low value of Md generally not present martensite transformation under mechanical stress. Another factor helping the forecast of martensite formation, is the value of the stacking fault energy (SFE), that is calculated like Md from the composition of the steel. This value is related to the ability of the dislocation to glide into an intersecting slip plane in a crystal. If this value is low, the mobility of the dislocations in the material decrease and the metastability of austenite increase so, low plastic deformation it is enough to have the austenite-martensite transformation, instead if is high, the austenite is more stable and the deformation occurs mainly by twins. The formula of SFE is the following, developed by Schramm and Reed: ***SFE (mJ/m^2)=-53 + 6.2%Ni + 0.7%Cr + 3.2%Mn + 9.3%Mo.*** [22]

The calculation of these two factors can give us immediately some important information. The high presence of molybdenum an nitrogen in the steel under investigation lead to quite nets outcome that will be confirmed later by the magnetic tests.[7][8][22][30]

1.4 Secondary phases precipitation

The big attention given to the thermal treatments, to the welding and to the exact service temperature, is due to the great tendency of the precipitation of secondary phases. This is because the duplex structure is thermodynamically stable from the melt continuing the solidification process until about 950°C. Below this temperature begin to became stable the σ and the Cr_2N phases. The isothermal section in fig.5 show how the austenite, σ and the Cr2N are consider, for the SAF 2507, thermodynamically stable at 800°C. Anyway, several secondary phases can precipitate on the DSS in the range temperature 300-1000°C. Into this range there are two main intervals where the precipitation works hard. The first is the so called "475°C transformation" (it occurs mainly between 475 and 280°C) where the spinodal decomposition occurs, it consists in a demixion of the ferrite in high and poor chromium contents in a very small scale. A subsequent hardening and embrittlement of the ferrite is observed. The duplex steels are sensitive to this phenomena, this should be enough to explain why most of the applications are restricted to temperature lower than 250°C.

The second main range is the 900-650°C which the ferrite is no more thermodynamically stable. Here occurs the eutectic decomposition of the ferrite that transforms into σ phase and γ_2 phase. χ, that is often observed as an intermediate precipitation before the formation of sigma phase from this. Unfortunately it is well know that the σ phase precipitate in all the DSS, but this is even more pronounced in the Super DSS because the high content of molybdenum and chromium move the formation curves of σ and other phases toward left (e.g. a less time for their formation). Moreover, it is established that the molybdenum enlarge the stability range of the sigma phase to higher temperatures. The sigma phase, usually represented with $[FeNi]_x[CrMo]_y$ plenty in Cr and Mo, is brittle, and affect the ductility both at high room temperature: a few percentage of sigma phase already reduce drastically the toughness of the steel even if the tensile properties are less affected, anyway the mechanical properties are worse than before the precipitation. Sigma is prone to precipitate in the duplex SS because it is thermodynamically stable at temperature below 800°. The diagram in figure 5, was calculated with *Thermocalc* (a

software that predict the stable phases in the range 800-1200°C in an alloy Fe-Cr-Mo-Ni) and the dotted line indicate the SAF 2507. Following that line from the top to the bottom it is possible to see that, starting from liquid, it begins to solidify the ferrite, then there is the big interval (1300-950°C) where ferrite and austenite are stable together. After 800°C the only phase stable are sigma, Cr_2N (showed as ε), and austenite.

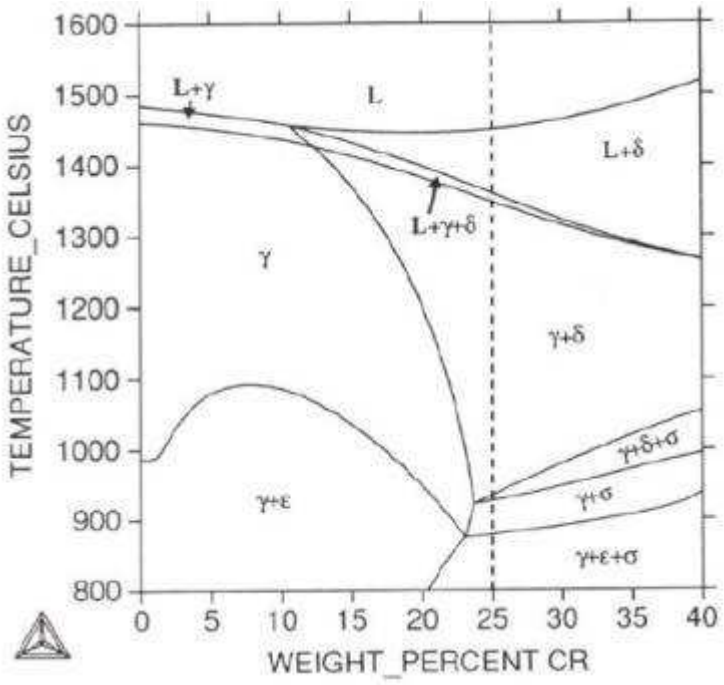

Figure 5 Computer calculated state diagram above 800°C, the dot line represent the SAF 2507.

Of course this not correspond perfectly to the reality, because the software does not take account of the diffusion rate (the diffusion rate in the ferrite is 100 time faster than in austenite) or the different dimension of the interstitial atoms and their difference in diffusion rates respect to the sustitutional atoms (Cr, Ni, Mo etc.). So, sigma is thermically stable under 800°C, but only with quite long stops, under this temperature is possible to obtain the precipitation of sigma.

It has to be considering also the corrosion resistance, very important aspect in this steels, indeed after the eutectic decomposition of the ferrite the steels shows a decrease in the corrosion resistance, some experimental data certainly shows that the secondary austenite decrease the average properties, particularly, is pronely to give pitting corrosion. The secondary austenite starts, because of the equilibrium volumetrically

fraction increase lowering the temperature, having quite the same composition of the primary austenite, it is difficult to differentiate from this one.

Precipitation of brittle sigma phase has of course be avoided. But it has to be strictly controlled the composition and the cooling rates after casting and every thermal treatment. Experimental investigation shows that the critical cooling rate to achieve 1% of sigma phase in the 2507 SDSS is 0.4 [K°/s] starting from a solubilization temperature of 1060°C. In figure 6 a diagram shows a curve to prevent the precipitations of secondary phases, and the way the solution elements modified the area of the formation of phases. The higher "nose" belongs to the sigma phase but is not the only one, other phases can coexist and it is difficult to separate the contribution; while the "bay" below represents the interval between the sigma phase precipitation and the 475 transformation area. However, it is possible to avoid the precipitation of phases; high cooling rates can lead to steels free of sigma and other phases. Unfortunately the increase in cooling rates facilitates the precipitation of Cr_2N, but with the right adjustments (e.g. simultaneous increase in Cr, decrease of Mo and increase of Ni) is possible to have a superduplex grade with higher structure stability.

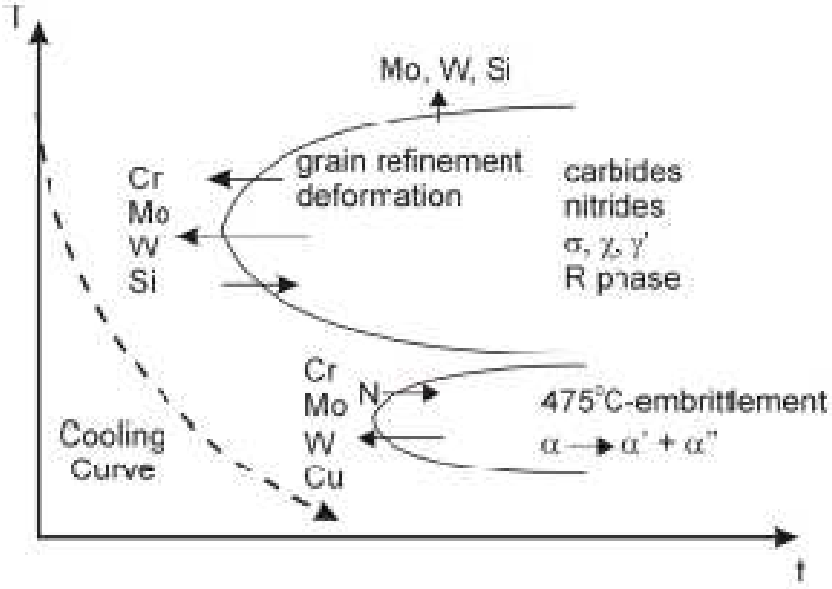

Figure 6: effect of chemical composition and cooling rate on the range of occurrence of various precipitates

The other phases that can precipitate apart σ,χ Cr_2N and γ_2 are some different kinds of carbide $M_{23}C_6$ even if the presence of carbide is very uncommon; there are also the R and π phases, rich in molybdenum, found in SDSS but these are less important, mainly because their formation kinetic is very slow, more than any treatment or process. [22][24][7][12][9][13][11][15][37]

1.4.1 The plastic deformation and the influence on the precipitation of σ phase.

As known, undergoing a plastic deformation in steel increases the amount of internal energy, which depends of the rate of deformation. Also, the yield and tensile strength increase.

For the duplex steels the analysis is not so simple, because they are polycrystalline materials composed by two different phases, one is the b.c.c. ferrite and the other is the f.c.c austenite. The first is more resistant, and has less slip plane and requires an high critical stress (τ_c) to activate the first slip plane, e.g. the one with the higher Schmidt factor (for example the {110} for the ferrite). For the second one, it is required a lower activating stress so, is easier to deform.

Steel is a polycrystalline material and the total effect on the final microstructure is the sum of the different behavior of the several crystals but also of the dimension of these.

It is possible to observe in the polycrystalline materials subjected to plastic deformation, 3 different types of microstructures: the number 1 that is similar to those for the monocrystal with a τ-γ curve in 4 steps. The second type is a net of equiassic cells separated by high angle edges. The third, where the large boundary of the cellar substructure (GNB) are totally misaligned respect the slip plane, while in the first type the GNB were aligned parallel between them and also with the slip plane.

The structure 3 and 2 should be typical for the duplex steels because it develop respectively on 3 and 4 slip planes, and deforming two phases surely, there is not only one slip plane. The type 3 crystals show a τ-γ curve that is parabolic (taylor) instead the type 2 crystals show a τ-γ curve with a rapid hardening at the beginning, that decrease the speed continuing the deformation. The GNB give a great contribution to the texture, because they stop only certain dislocations; and in the duplex with a little deformation it is possible to see a strong texture and grain refining.

There is another important thing that is the recovery that takes place at high strain rate, when a high number of dislocations and those with opposite burger vector can eliminate each other. This happens only into the cells because the boundary structure (stacked dislocations) is stable with a low energy level respect to within the cells; besides the speed of dislocations stacking decrease but does not stop, indeed continuing to deforming there is the formation of new border into the cells and consequently a grain refining.

In addition, the speed of hardening it is important for the composition of the alloy, it is a solid solution and the solute atoms easily act as nucleation centers especially with Frank-read mechanism.

To ensure the precipitations of sigma phase two thermal treatment were carried out in this work, at temperature where usually recovery and recrystallization starts under certain conditions. The recovery let move the dislocations that annihilate collapsing at the sub grain, high angle cells favoring the formation of new low angle grain borders. However, the effects of recovery are not visible at OM or at the SEM because, the microstructure remains the same, only the hardness may decrease slightly.

Recovery is an “internal energy consumer” it depends on the temperature, deformation rate and time. With high levels of deformation is difficult to notice a great effect of recovery that works anyway especially with high SFE materials like the SDSS, decreasing the dislocation density into the cells favoring the annihilation and the formation of new sub grains boundaries.

Recovery can eliminate the successive recrystallization step, because it can consume a great quantity of internal energy, which is the power of the recrystallization. Therefore recrystallization and recovery are two phenomena always in competition.

Sigma, as was mention first, is a hard brittle and non magnetic intermetallic phase with a tetragonal crystal structure. Sigma normally starts to grow at the ferrite/austenite boundary and continues growing into the ferrite grain in the form of a cellular structure, which consist in the sigma phase and new austenite. However, it grows also into the austenite grains but later respect into the ferrite; this is not only due to the fact that the ferrite is closer to the sigma phase in chemical composition, but primarily because of a higher diffusion rate on the δ phase.

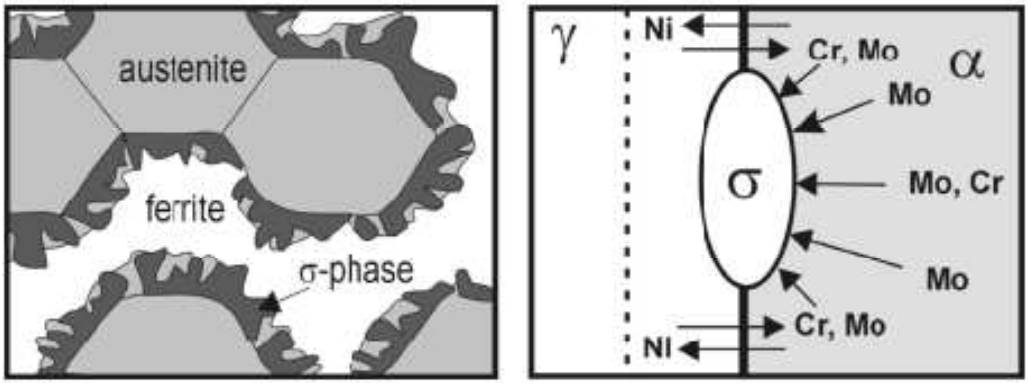

Figure 7 schematic diagram of sigma phase nucleation at the ferrite/austenite interface and its increase in the ferrite

Any processes that lead to a refine of grains e.g. increase the number of borders and the precipitations of sigma phase.

Generally the authors that analyzed the behavior of the eutectic composition in the DSS, concluded that a preceding cold deformation causes an acceleration of the ferrite decomposition $\delta \rightarrow \gamma_2 + \sigma$ [27][22][30]. In the work of Nenno et al.[18] has been investigated the effect of the plastic deformation on the precipitation of sigma phase. They found that in austenitic stainless steel cold rolled at 20%, cell structure and twins crossing remain stable also for temperatures of 550°C. Proved also that sigma phase after 3 hours at 700°C, precipitate at stacking faults, especially at the ends of these, and then grows; sigma was found also precipitate at the intersection of two twins of different orientation after

10 hours at 700°C; and also in the regions crowded of dislocations, that, after precipitation continues to crowd at particle border.

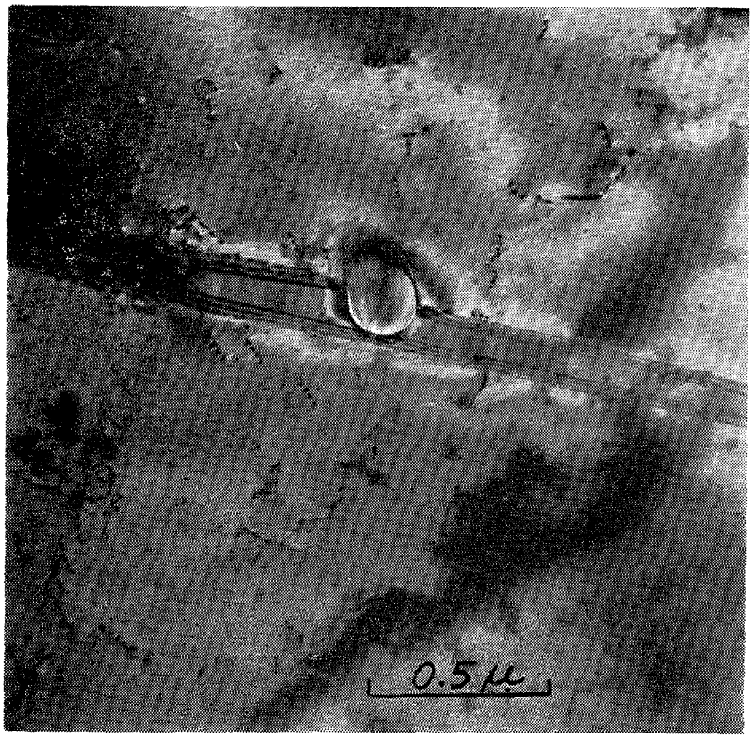

Figure 8: Sigma phase precipitated at twin boundary [18]

Unfortunately it has to be explained if there is really an acceleration, or if the nucleation starts before the conventional times (without cold deformation). [18][19][23][26][21][27][30][37]

CHAPTER 2

Sample preparation and OM and SEM analysis

The work of this thesis was done in collaboration with the University of Padua, Department of Engineering's Chemical Processing, and BME of Budapest, Science and Engineering Material's Department. The cold rolling and the XRD were carry out entirely in Padova, while the samples preparation (cutting, mounting and etching), metallographic analysis (Optical Microscope) were carried out in Italy and Hungary. The Magnetic Measurements in order to reveal the presence of martensitic phase, SEM-EDS-BSD-SE, EBSD, Micro-Hardness test and the two thermal treatments were performed entirely at BME of Budapest.

2.1 Sample preparation

The original bar of SDSS was supplied by the AvestaPolarit; it was hot rolled and annealed. The complete bar, was cut in 7 little pieces, which, except one (the as received sample) were then cold rolled in perpendicular direction to the original grain orientation (due to the weak hot rolling and continuous casting). The bar was deformed with a simple double-cylinder mill, able to deform the work-pieces with a speed of approximately 0.03m/s. The diameter of the cylinder is approximately 130mm. The 7 thicknesses reductions were the followed: 0% - 10% - 25% - 35% - 50% - 65% - 85%. Except the 10 % the other reduction was done with many passages.

Every little cold rolled bar (every specimen) was then cut to achieve 2 little pieces. These 2 little pieces of each sample (total 14 pieces) were mounted into the resin, in the way to allow the analysis of the transversal and perpendicular side, towards the rolling direction. This was made also to facilitate the grinding and polishing stages, and Optical Microscope, SEM and hardness tests analysis.

For grinding, SiC abrasive papers with decreasing particle size (220, 320, 500, 800, 1000, 1200, 2400) mesh were used, and for polishing clothes

with diamond paste (6 μm, 3μm and 1μm). These operations have to be carrying out carefully, without harden or overheat the material.

2.2.1 Etching

Is not possible to do metallographic analysis after polishing, because the sample surface is like a mirror. Therefore, it is necessary to etch the samples surface with a chemical solution in order to distinguish all the different phases. The way to see the true microstructure is choosing the best reagent that reveals the interested phases or constituents into the material, because the etching results strongly depending of the composition of the phases. For etching the samples, ***Beraha*** reagent was used: 100ml H_2O, 20ml HCl, 1g Potassium metabisulfite. This attack makes the ferrite phase no more planar, so it is presented as the dark phase at OM; and the white phase will be austenite.[7][9]

2.2 Analysis at OM

Optical Microscope technique is the common first step for analysis of metallic materials, considering that examines the material structure. It also allows seeing which phases are present, their quantity, their size and distribution. Therefore, OM technique is the first step to be taken in order to learn which material is working with. This technique let have a previously knowledge about the presence of materials defects such as porosity, non-metallic inclusions or cracks, and it is also very useful in order to evaluate the effect that external processes, such as heat, thermo-chemical and thermo-mechanical treatments, hot and cold plastic deformation could be on the material. The analysis was done in Padova with Leica DMRE Optical Microscope, in Budapest with OLYMPUS PMG 3; both OM worked with 100, 200, 500 and 1000X of magnification on longitudinal and transversal cold-rolled directions.

In theory Duplex Stainless Steels should have a 50/50 austenite/ferrite phases balance, but these values can change into a range (it is also possible to have duplex with 70% of ferrite and 30% of austenite). So, it is required a measure to know the correct phases distribution. This is the reason why it is necessary to perform an austenite/ferrite volume

fraction analysis. This analysis was done on as-received material etched with Beraha reagent.
The Image analysis was performed on ten different micrographs for every sample (5 transversal and 5 longitudinal respects the rolling direction). The magnification was 200x for the first 5 specimens (0%, 10% and 25%), while for the last 2 was used a magnification of 500x and 1000x, this because at only 200x of magnification, with a very fine microstructure to analize, the discrimination of the phases was very difficult. Anyway, greater is the magnification greater is the quality of the picture but the measure field now is very small and the analysis became microscopic. They were analyzed with "Image-Pro Plus v3.0 for Windows 95/NT", Media Cybernetics (1993/97) software. The are the following steps:

- Image capture
- Grey scale conversion of the picture (this software can detect 256 grey level, while the human eye only 50).
- Picture elaboration (brightness contrast etc.)
- Convert in binary file and segmentation (selection of the grey level)
- Pixel measure
- Results analysis

The analysis performed by the operator is very dependant to his evaluation of gray scales and his setting of brightness, contrast, filters of each photo; so, this analysis is strongly operator dependent, more, if there is a surface analysis that cannot give the exact phase ratio of all the bulk sample.
Fortunately other instruments gave us several phase analysis, and in the last chapter there is an interesting comparison of these. [9]

2.3 Electron scanning microscope

The Scanning Electron Microscope (SEM) is an electron microscope, that investigates the samples surface, scanning with an high-energy (30KeV) beam of electrons focused by condenser electromagnetic lenses to a spot about 0,4 to 5nm. The interaction between the electrons of the beam and the samples atoms generates some signals that allow revealing

information such as external morphology (texture), chemical composition, crystalline structure and orientation of materials making up the sample.
When the beam strikes the sample, the energy is dissipated as different signals, produced by the interactions between beam and sample. These signals include Secondary Electrons (generated with energies lower than 50eV by inelastic scattering at few nanometers inside the sample surface, and for this reason used to analyze the surfaces topography), Backscattered Electrons (BSE), Diffracted Backscattered Electrons (EBSD - were used to determine crystal structures and orientations of metals phases and textures), Energy Dispersive X-ray Spectroscopy (EDS - characteristic X-rays used for elemental investigation), visible light (Cathodoluminescence-CL), and heat.
Secondary electrons are most valuable for showing morphology and topography on samples, and backscattered electrons are most valuable for illustrating contrasts in composition in multiphase samples (i.e. for rapid phase discrimination).
All these signals were developed from different electron interaction volumes, and each signal has different imaging or analytical resolution. Those volumes depend on several factors, such as the energy of the incident beam (high energies increase the interaction volume, but they decrease the elastic scattering e.g. backscattering), the mean atomic weight (interaction volume decreases with lighter atoms) and the specimens density. Auger and Secondary images have the best imaging resolution, because respective electrons are generated in the smallest volume near the surface of the sample.
Backscattered electrons were generated over a larger volume, so, the images have intermediate resolution. Cathodoluminescence is generated over the largest volume, resulting in images with the poorest resolution. It is possible to choose the signal, and this depends on which information is looking for. After detection, the signal is amplified to create a variation of brightness on a display.
The raster scanning of the CRT display is synchronized with the raster scanning of the electrons beam, creating an image that is a distribution map of the intensity of signal emitted by the surface.

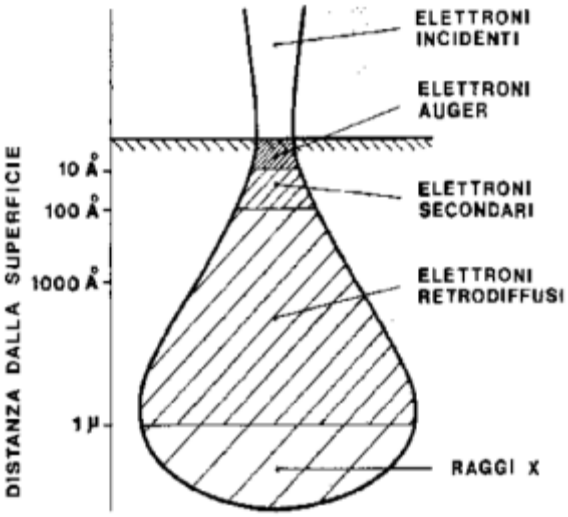

Figure 9 depth of the beam and provenience of the several scattered electrons.

The most important signals for scanning microscopy are the secondary electrons with lower energies, and re-emission or reflection of the high-energy backscattered electrons from the primary beam. The intensity of emission of both is very sensitive to the angle formed by the electron beam, when it strikes the surface to topographical features on the specimen.

Scanning Electron Microscope works at high voltage (about 29kV), and it is possible to reach a wide range of magnifications, from 10 times (about equivalent to that of a powerful hand-lens) to more than 50000 times. All the SEM analysis was carried out in Budapest with a PHILPS XL30. [7][9][36][44]

2.3.1 Back scattered electron

The Interaction of an accelerated electron beam with a sample target produces a variety of elastic and inelastic collisions between electrons and atoms within the sample. Backscattered Electrons (BSE) consist of high-energy electrons originated in the electron beam. These are backscattered out of the specimen interaction volume, by elastic scattering interactions with specimen atoms. Larger atoms (with a great atomic number) have high probability to produce elastic collisions because of their great cross-sectional area. Therefore, the number of backscattered electrons (BSE) that reach a BSE detector is proportional to

the mean atomic numbers of the sample. So, it is possible to obtain a high-resolution compositional map of the investigated surface with brighter areas given by atoms with great average Z (ex Mo), and darker areas where the average Z of the low atoms, and to provide information about the distribution of different elements in the sample and distinction of different phases.

Contrast Image depends on many electrons the detector is able to collect. With a normal detector these image properties are not excellent because the BS Electrons leave the samples surface with the same direction of the Incident Beam, and only a little amount of them is emitted into the solid angle subtended by the detector. It is possible to increase the current, increasing the beam energy and the average number of electron emitted by the surface, but this would decrease the resolution around 0,3μm (very low if compared with 20nm of Secondary Electrons). Therefore, the Everhart-Thornley detector, which is normally positioned on one side of the specimen, is not efficient for backscattered electrons detection. Hence, there are special backscattered electrons detectors positioned above the sample in a "doughnut" type arrangement, concentric with the electron beam, maximizing the solid angle of collection.[44][9][38]

2.3.2 EDS

Interaction of the primary beam with atoms in the sample can cause shell transitions which results in emission of X-rays. The emitted X-ray has an energy characteristic of the parent element. Detection and measurement of the energy permit elemental analysis (Energy Dispersive X-ray Spectroscopy or EDS). For this purpose a detector is used to convert X-ray energy into voltage signals; this information is sent to a pulse processor, which measures the signals and passes them onto an analyzer for data display and analysis. EDS can perform qualitative and semi-quantitative microanalysis of elemental composition on a specimen, with a sampling depth of 1-2 microns, from a relatively low (~25X) to high magnification (~20000X).

The electron beam have an average diameter of 1μm, thus, tiny particles cannot be analyzed precisely because some data by the material close to

the particle giving an incorrect pattern of composition. Nevertheless, the emission depth is about 1-2 microns, it means that if the particles analyzed is very thin (<1micron) the XRay's beam size is like the particle size, and this lead to collect also information not only from the particle but also from the surroundings. So after collecting the spectrum the operator have to be very carefully. [44][7][38]

2.3.3 EBSD

Electron Backscatter Diffraction (EBSD) is a technique which allows crystallographic information to be obtained from samples in the SEM. In EBSD a stationary electron beam strikes a 70° tilted crystalline sample (to optimize the contrast in the diffraction pattern and the fraction of electrons scattered from the sample), and the diffracted electrons form a pattern on a phosphor screen which is fluoresced by electrons from the sample to form the diffraction pattern.

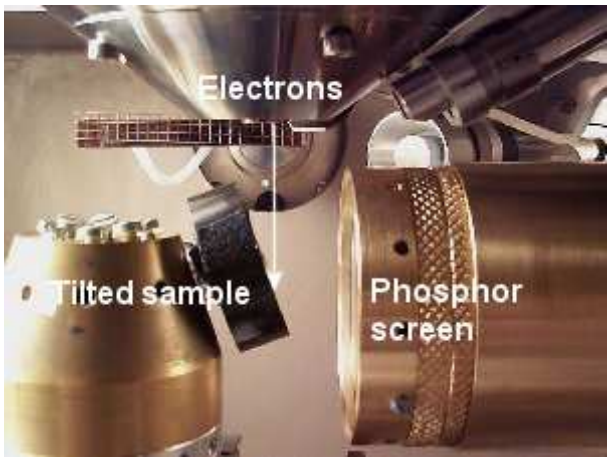

Figure 10 picture of the internal disposition of the SEM component

This
pattern is characteristic of the crystal structure and orientation of the sample region from which it was generated. The symmetry and appearance of the pattern is related intimately to the crystal structure, at the point where the beam meets the sample. If the crystal rotates (in

other words the orientation changes) the diffraction pattern will be moved. If a different type of material is placed under the beam, the diffraction pattern will change completely. The diffraction patter is formed after the beam strike the sample; the atoms in the material inelastically scatter a fraction of the electrons with a small loss of energy to form a divergent source of electrons close to the surface of the sample. Some of these electrons are incident on atomic planes at angles which satisfy the Bragg equation:

$$n\lambda = 2d * sen\theta$$

Where n is an integer, λ is the wavelength of the electrons, d is the spacing of the diffracting plane, and θ is the angle of incidence of the electrons on the diffracting plane. These electrons are diffracted to form a set of paired large angle cones corresponding to each diffracting plane. When is used to form an image on the fluorescent screen, the regions of enhanced electron intensity between the cones produce the characteristic Kikuchi bands of the electron backscatter diffraction pattern.

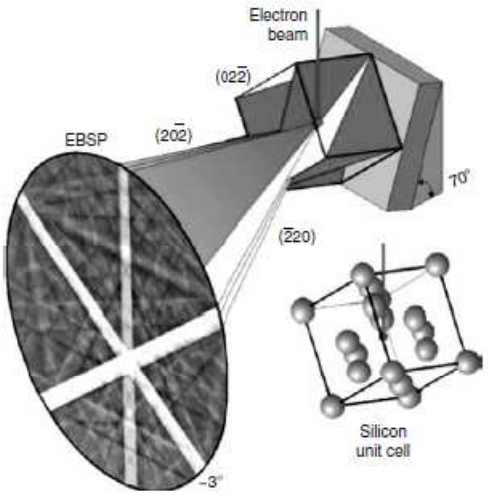

Figure 11. Electron interaction with crystalline material (Si), how the kikuchi lines forms. [34]

The centre lines of the Kikuchi bands correspond to the projection of the diffracting planes on the phosphor screen. Hence, each Kikuchi band can be indexed by the Miller indices of the diffracting crystal plane, which formed more a Kikuchi large band that correspond to a high *d* (distance between planes) and viceversa. Each point on the phosphor screen corresponds to the intersection of a crystal direction with the screen. In particular, the intersections of the Kikuchi bands correspond to the intersection of zone axes in the crystal with the phosphor screen. These

points can be labeled by the crystal direction for the zone axis. The positions of the Kikuchi bands can therefore be used to calculate the orientation of the diffracting crystal. To do this, is necessary to know the band position, given by the Hough transform, that change the coordinates from *xy* to ρθ of the new Hough space where is possible to see the previous lines as points, because a straight line in the conventional space is characterized by ρ, the perpendicular distance from the origin and θ the angle made with the x-axis, which is represented by a single point (ρ, θ) in Hough space, also the height of the Hough points give the quality of the measure. Now it is possible to allocate the Miller index (system have a database of ρ, θ couples that immediately identifies the plane) and to calculate the orientation of the crystal lattice.

Therefore, the diffraction pattern can be used to measure the crystal orientation, identify materials, measure grain boundary misorientations, discriminate between different materials, and provide information about local crystalline perfection. When the beam is scanned in a grid acrossed the polycrystalline sample, the crystals orientation measured at each point will reveal the constituent grain morphology, orientations, and boundaries. This data can also be used to show the preferred crystal orientations (texture) present in the material.
One of the most widely used features of the EBSD is to carry out the phase map of the sample, here for example is possible to clearly see the different phase and their percent, indeed in this map it is also possible to see the orientation of each crystal, colored according to the Inverse Pole Figure that act like a legends. The IQ map is also important, in the grains and subgrains border the kikuchi lines are not so clear as in the center because here there is concentrations of defects, therefore, the height of the Hough points will be shorter and it correspond to a darker pixel in the IQ map. This technique was used in this work to show that the areas of formation of the new sigma phase have a lower IQ, that means that tension and stresses were rise in that areas. Other interesting features are the measuring of distribution of grain sizes, that can be calculated from the data collected for the map. In addition, the distribution of grain

boundary misorientation angles and the distribution and position of special grain boundaries can be shown.
But there is great use of EBSD for calculating the texture, the individual crystal orientation measurements collected by crystal orientation mapping can be used to show the crystallographic textures developed in the sample, the various textures in the sample can be separated automatically, their volume fractions calculated, and the regions of the sample which they originate shown.
An interesting work [25] used the EBSD for calculate the stored energy in each grain starting from the height of the peaks of the Hough transform.

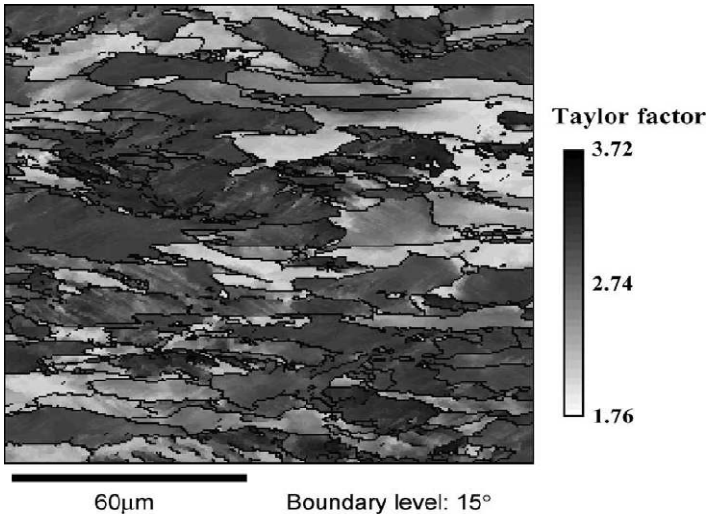

Figure 12. Spatial distribution of Taylor factor (directly proportional to the stored energy) in which the gray level is proportional to the local stored energy [25]

The beam has to focus on the surface sample, then the electrons beam strikes the surface, and electrons of all energies are scattered from the sample to the detector that collect them to form a background to the diffraction pattern, which reduces the contrast of the Kikuchi bands. The background intensity can be removed to improve the visibility of the Kikuchi bands, besides, can be measured by scanning the beam over many grains in the sample to average out the diffraction information. The background can be removed by subtraction from, or division into, the original pattern. When is possible to see clearly the kikuchi lines one can regulate the accelerating voltage or the probe current; the first reduces the electron wavelength and hence reduces the width of the Kikuchi bands in the diffraction pattern .

Also, when more energy is being deposited on the phosphor screen, this will result in a brighter pattern, which requires a shorter integration time. Instead, increasing the second one will increase the number of electrons contributing to the diffraction pattern, and then the camera integration time has to be reduced. However, this must be balanced with the spatial resolution required, because increasing the probe current will also increase the electron beam size. Typical beam diameters at 0.1 nA probe current and 20 kV accelerating voltage are 2 nm for a FEG source and 30nm for a tungsten source. For this work the acceleration voltage was always 25KV. The beam profile on the sample surface will also be elongated in the direction perpendicular to the tilt. The spatial resolution achieved in practice will depend on the sample, SEM operating conditions and electron source used and under optimum conditions grains as small as 10 nm can be identified.

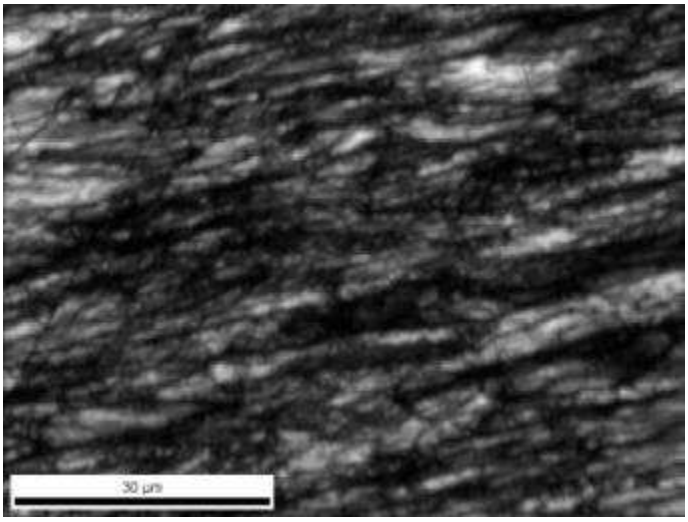

Figure 13. Example of a very bad image quality due to the stress in the material.

The sample preparation for use this technique requires more time than for a conventional SEM analysis, diffracted electrons escape from within only a few tens of nanometres of the specimen surface, specimen preparation for EBSD is critical to achieve good results. If the material near the surface is deformed, or has any surface contaminant, oxide or reaction product layers presented, then EBSD pattern formation may be suppressed. Therefore for this work, after the used polishing until 3μm, an additional one with 0.05 μm colloidal silica for 30 min were carried

out; this to ensure a very high surface quality, because this technique is strongly affected by the surface conditions.
After the picture collection, the EBSD create a file that needs special software to be elaborate to extract the several useful maps and information. This software permit the operator to decide to “clean” the figure, that means that the operator can decide the minimum grain size to keep in consideration from the software, after creating the phase map is possible to draw only the grain borders that have a misorientation higher than a set value. This and many other features permit to the operator to elaborate the images to obtain the desired information. The software used for this work was the ***TSL OIM Analysis 4.6***. [34][43][25][34][28][14][16][38][42]

2.4 Hardness

The hardness of a material is generally defined as the resistance that it opposes to the penetration of another body with specific geometry and with greater hardness, which moves slowly in perpendicular direction to the specimen’s surface with a certain load.
For this study all the Vickers Micro-Hardness Tests were done using “IndentaMet™ 1100 Series made by BUEHLERR” of the BME of Budapest with a load of 200g. The Vickers test has two distinct force ranges, micro (10g to 1000g) and macro (1kg to 100kg), to cover all testing requirements. The indenter is the same for both range therefore Vickers hardness values are continuous over the total range of hardness for metals (typically HV100 to HV1000). With the exception of test forces below 200g, Vickers values are generally considered test force independent. In other words, if the material tested is uniform, the Vickers values will be the same if tested using a 500g force or a 50kg force.
The full load is normally applied for 10 to 15 seconds.

The indentation shape cannot be perfectly square, because of the different hardness of ferrite and austenite, so in the measures of the diagonal there could be a little error.

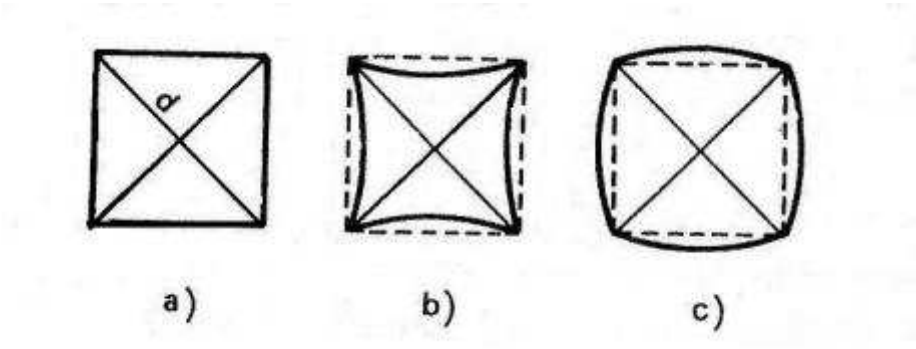

Figure 14 indententation shapes.

In the figures can be recognized the classical shapes of the indentations, indeed is rare that the indentations are perfectly square a). The most widespread is the b) with often not equal diagonals that are the characteristic indentation shape for the hardened material. Is characteristic because the material consist in two phase, one, the ferrite, that is stronger therefore more difficult to deform. The other phase is the softer austenite. So, indenting half ferrite grain and half austenite grain, the indentation shape will surely result strange with an indentation that may have the shape of a 4 point star because of the springback of the material. [10][7][9]

2.5 X-Ray diffraction

Every crystal lattice is made of a number of atoms that are arranged, to form a series of parallel planes separated from one another by a distance *d*, which varies according to the nature of the material. For any crystal,

planes exist in a number of different orientations - each with their own specific *d*-spacing.

The principle of the machine is that an X-ray beam hit the sample. X-rays are electromagnetic waves with $\lambda<\lambda_{visible\ light}$ produced whenever high-speed electrons decelerate rapidly by collision with a metal target. X-ray monochromatic radiation is generally generated into a x-ray tube which has an electrons source and two high d.d.p. metallic electrodes. If electron incident beam has enough energy to be able to eject a K electron from an atom of the target, one electron from outer shells immediately falls in space remained available, and the atom emits a quantum of defined wavelength greater than the wavelength of incident radiation. When this monochromatic X-ray beam with wavelength λ is projected onto a crystalline material at an angle θ, diffraction occurs only when the distance traveled by the rays reflected from successive planes differs by a complete number *n* of wavelengths (called constructive diffraction).

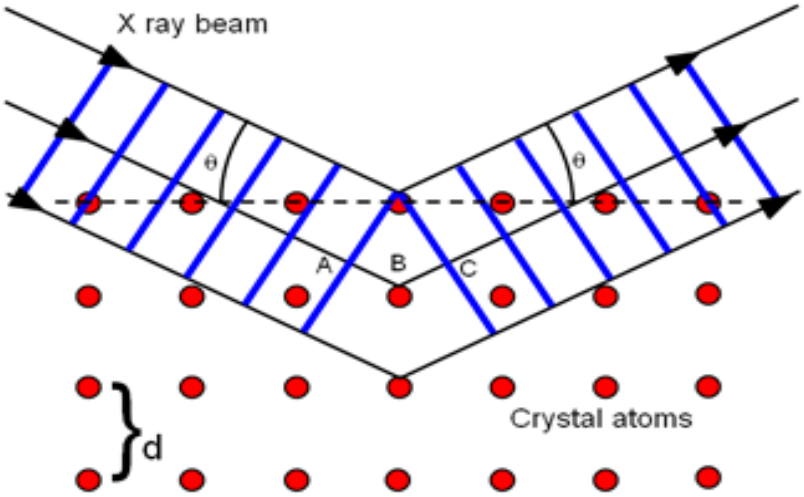

Figure 15: how the x-rays can be reflected by the crystal planes.

This instrument is based on the well know Bragg's law: $\lambda = 2d \sin\theta$. By varying the angle θ the Bragg's Law conditions are satisfied by different *d*-spacing in polycrystalline materials. Plotting the angular positions and intensities of the resultant diffracted peaks of radiation produces a pattern, which is characteristic of the sample. Where a mixture of different phases is present, like the case of the duplex steels, the resultant diffractogram is formed by addition of the individual patterns.

X ray diffraction is a surface technique, so the information comes only by the surface, which has to be former prepared with a polishing until 2400 mesh.

Anyway XRD revealed useful in some recent works on SAF 2205 to evidence the presence of martensite after cold rolling [7][10]. Anyway, this technique presents several limitations like when the crystal's repeating unit, this unit cell becomes larger and more complex, the atomic-level picture provided by X-ray crystallography becomes less well-resolved (more "fuzzy") for a given number of observed reflections. [7][9][41][10]

CHAPTER 3

Magnetic investigation

3.1 Magnetism and its different classifications

In our life was been used and worked with many materials. Most of this does not show particular behavior under the effect of a magnetic field. The rest of this, under the application of a magnetic field shows different effects: from the attraction to the repulsion. There is also a category of natural material that shows magnetic property and some material can remain magnetized after the application of a magnetic field. In the following paragraph the principle of the magnetism and the main effects on the material, especially the one called Ferromagnetism (the more important and widely used) will be descript.

To describe the magnetism it is necessary to introduce various quantities. Starting from H that is the field applied; B instead, the field generated into the material after the application of H, is defined as:

$$\boldsymbol{B} = \boldsymbol{\mu_0} * (\boldsymbol{M} + \boldsymbol{H})$$

Where μ_0 is the vacuum permeability and M is the magnetization, i. e. the contribution of the material at the field generated; M describes directly the magnetic property of the material. Other parameters are the relative magnetic permeability $\boldsymbol{\mu_r}$ and the susceptibility$\boldsymbol{\chi}$, they are linked with:

$$\boldsymbol{\chi} = \boldsymbol{\mu_r} - \mathbf{1}.$$

χ gives an idea of how much the material is influenced by the magnetic field. The total magnetic moment of an atom is due to two sources: the first is the orbital motion of the electron around the nucleus (assimilated to close circuit current) and give the magnetic orbital moment; the second is due to the fact that each electron has their own spin and related to this, there is an intrinsic magnetic moment. It has to say that the macroscopic properties of material are strongly influenced by this magnetic moment associated to each electron running around each atom. However, each atom or molecule of the material acquire, under the application of an external magnetic field, an average magnetic moment <m> oriented parallel to the field B. Taking this average <m> , with Δt a little volume

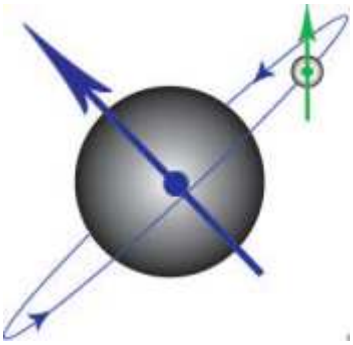

Figure 16 Magnetic moments produced by an electron orbiting the nucleus and that produced by the spin of the electron.

of material and ΔN the number of atoms into this volume; it is possible to write the magnetization M as

$$\boldsymbol{M} = (\boldsymbol{\Delta N}/\boldsymbol{\Delta t}) * < m >.$$

It is possible to write M also with $M = \chi * H$. Now is clear that χ can measure how much a material magnetize itself under a magnetic field. χ can vary from 10^{-5} A/m (soft magnetic material) to 10^{-6} A/m (hard magnetic material).

On the diamagnetic substances the μ_r is constant and independent from B and <1. In this case the amperian currents give an opposite contribution so, the magnetization will be opposite to H, and anyway also with very strong field the magnetization generated is very weak. Without the application of an external magnetic field there are any magnetization effects, because all the magnetic moments are compensated and in each atom the total magnetization is 0. Susceptibility in this kind of material is small and negative, for the solids are of the order of 10^{-5}; some examples are the gold and the lead that can reach $-1.58*10^{-5}$.

In some substances, there is an asymmetry condition: is the case of the paramagnetic ones where there is not compensation of the magnetic moments (due to the electron and to the spin), and therefore each atom has an intrinsic magnetic moment. In absence of external magnetic field H, the total moment result zero, this is because the termic agitation that shake the atoms. But when an external magnetic field H is applied, there is a partial orientation of the moments (always disturbed by termic agitation) that give a magnetic moment <m> aligned to H, proportional to him and inverse proportional to the temperature. Anyway at temperature room the magnetization is little; is the case of the aluminum where the

susceptibility is $2*10^{-5}$. For this material the susceptibility χ is little but more than zero. And for the diamagnetic, turning off the external field the total magnetization moment return to zero.[2][3][1][7][40]

3.2 Ferromagnetic materials

The properties of these substances are very different from the others. Ferromagnetic materials are the most interesting materials for work with the magnetism. Unfortunately for the ferromagnetic materials there is not a classical explanation of the phenomena, it is necessary a quantistic explanation, anyway, there is a particular condition in each atom where the intrinsic magnetic moment is mainly due to the electron spin. These are not compensated each other, there is quantistic interaction between them. It is possible to see it in the following modified formula for the field B:

$$\boldsymbol{B = \mu_0 * (H + \gamma M)} \ .$$

That is valid locally. γM is the Weiss local field due to a mutual oriented action that align the m_0, favored by the reach of a state of minimal energy, it give, also with H=0 a magnetic moment M that can be greater than the previous H applied. This is the peculiarity of this kind of materials.

According with this positive interactions between magnetic moments, there are many small region, in a crystal of ferromagnetic material, called Weiss Domains, containing more than 10^8 atoms that have some magnetic

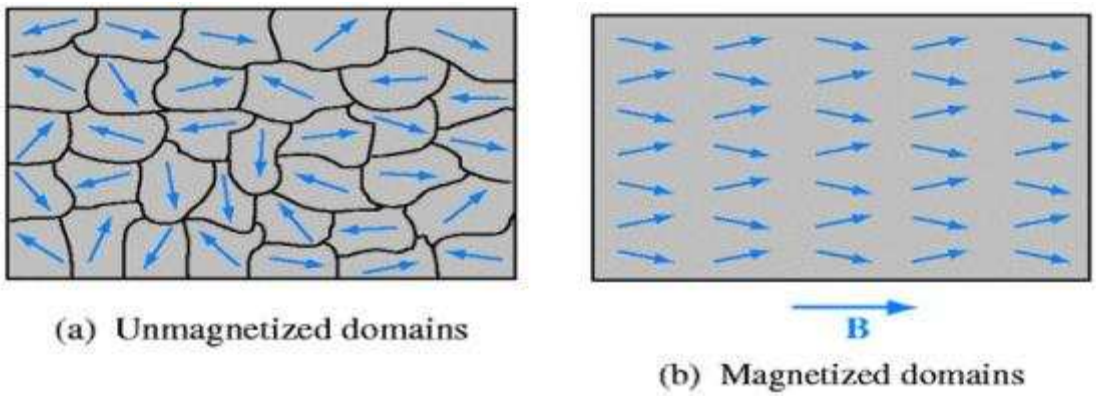

Figure 17 In (a) it is showed the start conditions of the domains, in (b) the situation is when an external field is applied.

moment direction (due to magnetic moment interaction that align the spins). Each domain has different magnetization directions and they are divided by “blocks wall”. Through those walls the magnetic directions change with continuity. Even if each domain is magnetized the total material can have M=0, because the domain are random oriented. As an external magnetic field H is applied, the block wall starts to move, modifying the domain size, there will be an increasing in size of those domains that have parallel magnetization to H, and consequently the domains where the M is not parallel will decrease in size. Increasing the external field all the remained domains will be aligned and the material will saturate.

The motions of the walls are not reversible due to imperfections and defects (such as dislocations) so, turning off the external field H will remain a residual magnetization. Indeed when more the dislocation density, would greater be the impedance to domain wall motion (this explain why the cold worked specimens have higher coercivity and lower initial susceptibility).

Due to the obstacles the domain walls movements has a discontinuous speed due to their interactions with pinning centers formed by microstructural defects such as dislocations and grain boundaries. These pinning centers block domain walls motion, until there is enough external energy to overcome local energy barriers created by the pinning center. When this condition is achieved, sudden changes in the magnetization are produced by the rapid movement of domain walls. These sudden movements can induce voltage pulses in a secondary coil placed near the material. These pulses can be “listened as noise” using an amplifier and a speaker. These step variations in magnetic flux are random and commonly called Magnetic Barkhausen Noise (MBN).

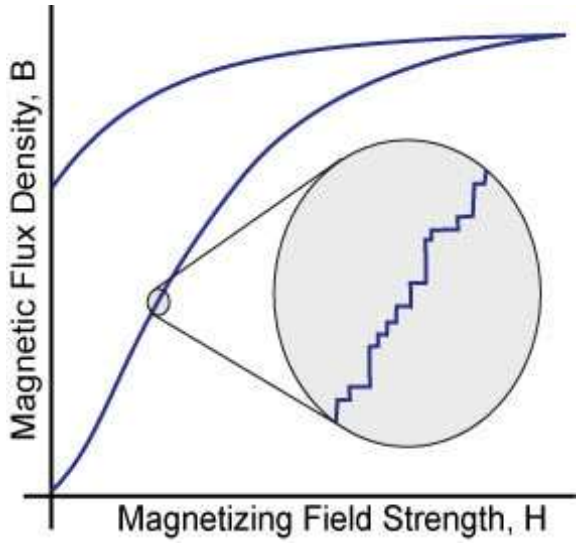

Figure 18 sudden movements of the domain walls represented on the hysteresis curve

Concluding, ferromagnetic

substances give very high magnetization also if the applied field is low. It is important to know that this property varies noticeable with the composition (also very little variation can delete the ferromagnetic properties) and with thermal treatment. Magnetic properties can also vary with deformation and mechanical stresses. So, the atomic phenomena that drive the ferromagnetism derive from the crystalline structure and his modification due to thermal or mechanical operation. Anyway these materials have $\chi>1$ and very high, typically from $\chi=50$ to $\chi= 10000$; example of this class of materials are: iron, cobalt, etc. [2][3][1][7]

3.2.1 Ferromagnetism and Hysteresis loop

For diamagnetic and paramagnetic materials there is linear relation between B and H. For the ferromagnetism this is not the case. Susceptibility and relative permeability (both positive and big) here depends from the H value and also from the way of increasing of it. The most important single property of ferromagnetic materials is their high relative permeability's. The μ_r is not constant; indeed in order to characterize the properties of a given ferromagnetic material, is necessary to measure the magnetization induction B as a function of H over a continuous range of H to obtain a hysteresis curve. Application of an external field H causes the magnetization induction B to rise, from 0 to a maximum value called magnetization saturation and that remain constant while H increase again (at which correspond $H=H_m$).

The field rises drawing the first magnetization curve *(a)*. After H_m the B fields arise again but of a very little rate, indeed relative permeability is very little. Now, H decrease until 0. The values of B and M lies in a different curve *(b)*, a new one that stay above the first magnetization curve and intercept the Y axis in a point called Br, the remain induction. Now the material is magnetize also without external filed applied, it is a permanent magnet. To reduce the induction to zero the applied filed must be reduced until Hc: the coercive field. Continuing to decrease H the situation is the same of the positive values, lower than $-H_m$ the magnetization curve stop to decrease and remain almost constant. Finally if the H values increase again until $+ H_m$ the magnetization follows the *(c)* curve to reach the magnetization.

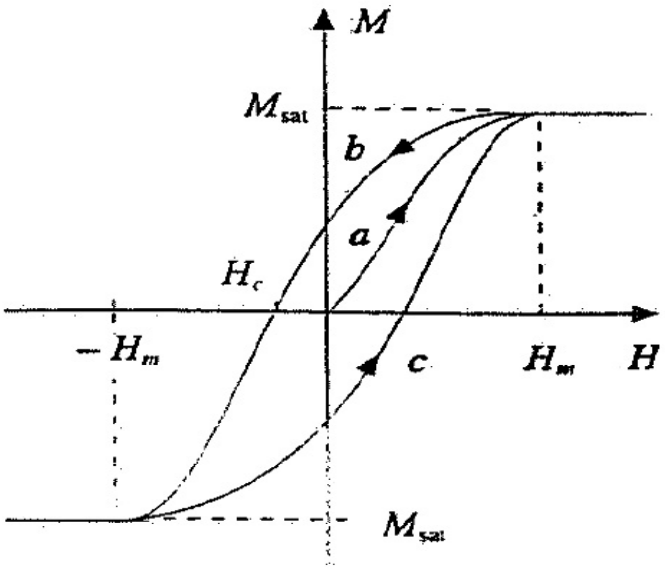

Figure 19: Saturation Hysteresis loop of a ferromagnetic material.

The condition that the material reaches at M_0, shows all the magnetic dipoles within the material aligned with the external magnetic field H. The saturation magnetization depends only on the magnitude of the atomic magnetic moment *m* and its number *n,* giving $M_{sat}=m*n$.
The hysteresis loop represents a state diagram of the material. The saturation loop is the bigger one, while stopping H before reaching H_m lead to draw an internal loop. Indeed a large loop is called "hard" and it is good for make permanent magnets while a thin loop is called "soft" and it is good for make electric magnets. Another important thing is the critical temperature Tc, which is specific foe each ferromagnetic material, and above this the material become paramagnetic. [2][3][1][7]

3.2.2 Magnetic behavior of γ and α

One important concept is to know why the phases of the same material have a different magnetic behavior. It is again connected to the quantistic relation between the electrons and atoms; to better understand the topic, the Bethe-Slater curve in the following picture is represent.

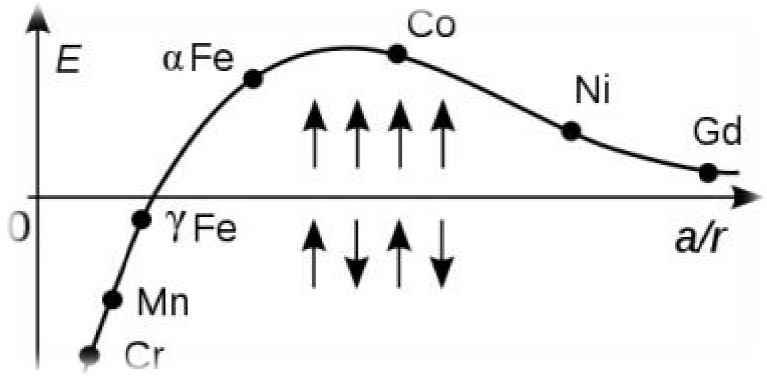

ile antiparallel lead to

The *E* showed in the graph is not about only the electrons; indeed it represents the variation of exchange energy *E* for transition metals as a function of the ratio of the interatomic distance *a*, to the radius *r* of the 3d electron shell.

This means that if two atoms of the same kind are brought closer together than *a/r* will decrease. When *a/r* is large, than *E* is small and positive; as the ratio decrease, *E* at first increases and then after reaching a maximum value decreases and finally become negative indicating antiferromagnetic order at small values of *a*. Taking in consideration that austenite is CFC and its APF is 0.74 and the ferrites one is 0.68 (atoms less packed). This means following the graph that in the passage $\alpha \rightarrow \gamma$ the a/r ratio decreases, therefore the J became negative leading to a antiferromagnetic behavior.

Originally the exchange energy *E* was calculated only about the electron of two non-filled neighbor atoms, it has no classical analog, indeed to find out it is necessary to consider a wave function where the terms related to the spins are fundamental: the result of this wave function is that, deriving from it the *E*, if the electrons have parallel spins the *E* is positive and hence corresponds to ferromagnetic order. [2][3][1][7]

3.3 Magnetic tests

Magnetic tests were widely used to analyze this steel. They are very useful for find any variation of ferromagnetic phase content in the material. The several information take out from the hysteresis loop was the following: Saturation induction, it is directly proportional to the trend of the ferromagnetic phase in the material, so if it decreases, the saturation induction decreases too. Remanent induction, it is proportional to ferromagnetic phase too but does not give a good correlation as the saturation induction. The coercivity, it is proportional to the hardness, especially on the carbon steel, caused by imperfections whether in the form of dislocations or impurity or new phases growth in the material.

In this work the following magnetic tests used were: a specially designed permeameter-type magnetic property analyzer, the Forster magnetometer, the Stablein-Steinitz test and the Fischer ferritoscope tester.

Unfortunately the tests were not carried out with the MBNT because of the impossibility of take out from the bars of steel the proper specimen, that require: width≈20mm, lenght≈120mm with thickness dependent to deformation rate. The fists two are AC tests while the others are DC tests. Ac tests differs from the DC for the more precision on the measurements unfortunately these tests are not able to supply strong magnetization field, indeed to achieve saturation in steel like the one under investigation is necessary to work with a DC instrument that supply very strong field, also because DC systems are free from eddy currents. Another difference between magnetic tests is that they can be open or close circuit. In the close circuits the specimen touches the surfaces of magnetic poles, therefore, there is no air gap and the magnetic field lines can perfectly pass through the specimen without theoretical losses. The things change for the open circuits, because here the sample does not touch the magnetic surface; there is an air gap thus now the shape and the size of the sample became very important because these depends the size of demagnetization factor. It is possible to write $H_{IN} = H_{OUT} - D * M$ where M is the magnetization of the sample, and D is the demagnetization

factor, it means the supplied field will be always higher than the field that really feels the sample.

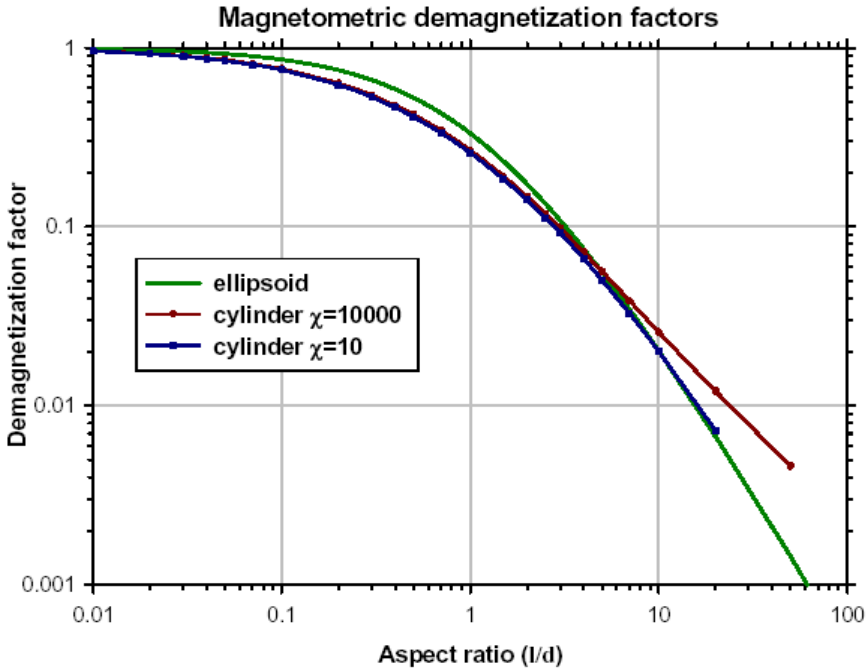

Figure 21 graph of correlation between aspect ratio and demagnetizing factor, with several shapes.

D is dependent on the geometry of the specimen; the sample used on the open circuit test in this work are parallelepipeds, these are equals to a cylinder of the same length (40mm) and same head-area that is 20mm^2 so, this cylinder have a diameter of 5mm and consequently an aspect ratio l/d of 8. According to the magnetometric demagnetization factor's graph, is possible to see that the correspondent D for a cylinder with aspect ratio of 8 is about 0.01÷0.02; therefore the measures were not so much affected by this problem.

Fortunately the sample investigated was elongated but if we had a coin, with magnetic poles close to each other the D was higher and consequently the field H_{in} was too much lower than H_{out}.

Unfortunately after cold rolling, especially for the hard rolled samples, there was a little bending. This is nothing but an additional plastic deformation (but of course, minor). In the magnetic tests, all the samples' volume is magnetized and the detector coil is around the sample. It was measured the total volume behavior; so is not important. But, in the AC instrument, due to the bending, there could be more space between the two soft iron yoke. This can lead to a shearing effect that is a change of

slope of the hysteresis curves, leading to a “flattening” of them, and influence the permeability and the remanent induction. [2][3][7][39]

3.4 Ferrite tester

The ferrite tester is an instrument used all around the world, as the name say, is an instrument for the measure of the ferrite content in the steel under investigation.

The ferritescope measures according to the magnetic induction method. A magnetic field generated by a coil enters into interaction with the magnetic components of the specimen. The changes in the magnetic field induce a voltage proportional to the ferrite content in a second coil. This voltage is then evaluated, then ferrite content measurements can also be carried out regardless of the substrate material properties starting at a plating thickness of 3 mm.

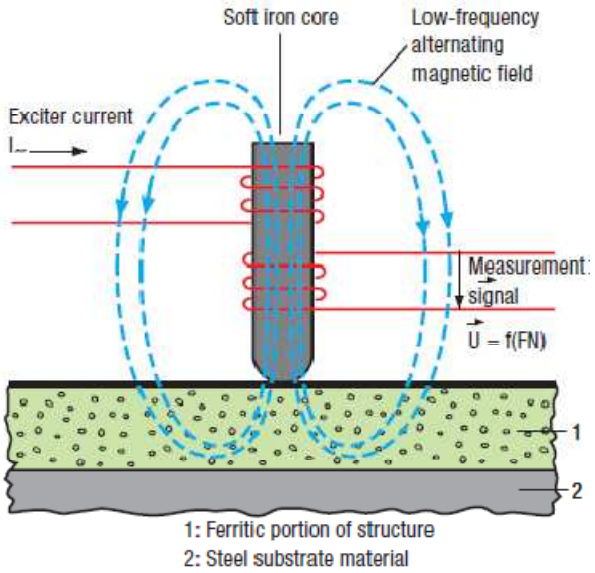

Figure 22 Schematic of the operating principle of the ferrite tester by Fischer

Unfortunately the producers of these instruments only give hints, like this, regarding the working of this device. However, there is a magnetic field, that should lead to saturation the ferromagnetic phases in order to reveal their quantity. Usually in the classical magnetic tests to saturate little specimens high excitation fields are required (ex: 1000 A/cm) they are supplied by a magnetizing coil plugged to industrial or home network (220V) and function generator. The ferritoscope being a portable

instruments use, instead of classical network, 4 normal AAA batteries each of 1.5V to generate the excitation field, the Fischer consider the field generated enough to saturate the ferrite, and the data are considered valid not only for the surface, but for the total thickness of the steel under investigation.

The data evaluated with this instrument are widely used, in conferences, scientific articles and others official documents. Therefore, some measures with the Fischer ferritescope were taken in the samples of SDSS under exam in this work. [45]

3.5 AC magnetization curves test

This open circuit magnetic test is a specially designed permeameter able to measure different values from hysteresis loop, such as *Saturation Induction* (*Bs*), *Remanence Induction* (B_R), *Coercive field* (*Hc*) and *maximal relative permeability* (μ_{max}).

The equipment consists of a 300 turns excitation coil in which is inserted the sample. Being the sample longer than the coil, to avoid the demagnetization effect 2 iron core flakes with good soft magnetic properties were applied, these 2 flakes increase the cross section and close the magnetic circuit with the specimen in the middle. All is connected to a function generator and a power amplifier. The function generator supplies a sinusoidal exiting current, which induces a magnetic field H in the sample. The signal detector coil is around the middle of the specimen, and it reveals the induction field B. Everything is connected to a PC computer in order to control and collect the measured data. The Pc is also equipped with an air gap compensation function to compensate the fact that the sample did not fill completely the whole size of the coil so; there is a space between coil and sample. The current supplied is a 5Hz current because with a higher frequency the eddy currents would be too much. The applied maximal effective field strength in the

magnetizing circuit was 19760 A/m to give some better resolution curves, while the number of measured point per cycle was 100. The specimens used for this test are very small; indeed the device used was not the classical one with “U” shape laminated Fe-Si iron yoke. Here, the samples consist in a little bar of 1.54mm width and 20 mm thickness. Unfortunately, due to the strong deformation, these samples were not completely flat, especially the most deformed was bend a little, the effect of this are decrypted in the beginning of this chapter. [7][2]

3.6 Försters magnetometer

Forster test is open circuit magnetic equipment used to reveal the real coercivity Hc value from the saturation hysteresis loop. It consist in a large solenoid coil which can produce 1000A/cm magnetic field (enough to magnetize the present steel) and two magnetic sensors which sensitivity is very high (~1nT).

The idea of this equipment is very simple and it is based to the definition of coercivity.

The specimen is put in the middle of a solenoid coil and it is magnetized up to the saturation by a slow increasing of the excitation field. After that, this excitation field made by solenoid coil must be decreased slowly until H=0. The sample contains some ferromagnetic phases, remains magnetized showing the own little magnetic field. The sensors, being the sample exactly perpendicular to them, are not able to measure the remanent magnetic field because the sensitivity direction of the sensors is perpendicular to the coil, and as long as the specimen remains in the middle of the coil, the perpendicular component will be zero.

Therefore, the second step consists on moving the sample horizontally in the coil until the sensors detect the maximum perpendicular component. These two components have same direction but opposite signs, therefore, the signals revealed by the sensors are subtracted from each other in order to increase the sensitivity to the double. The third step is, with the

sample leaved in the point of maximum field detection, to change the polarity of the coil and to increase very slowly in the opposite in order to achieve zero current detected (sample demagnetization). The exciting field required corresponds to the coercive force Hc.

This instrument takes care also of the magnetic field of earth, which in some case could influence the measures. The earth magnetic field is about 50μT, fortunately in the case of this samples the saturation is much more, about 0.6T, so we worked in a range where there is no affection by earth magnetic field. Anyway the system is tilted, to be in axis with the magnetic field of earth and there are two permanent magnet that can be seated to compensate this field.[7]

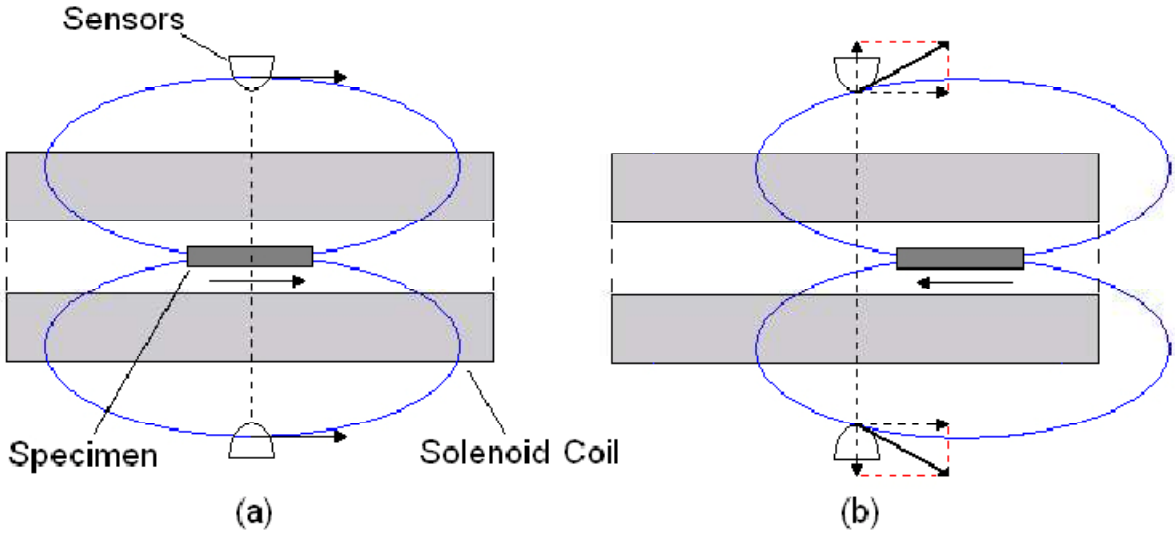

Figure 23: (a) when the sample is perpendicular to the sensors they detect only the horizontal component while the perpendicular is zero. (b) when the sample, that is magnetized is move out from the center, the sensor detect a inducted current until reaching the maximum value of this.

3.7 Stäblein Steinitz test

Stablein-Steinitz is a DC close circuit magnetic equipment designed to reach high coercivity and magnetization field with samples which have small length/transverse dimensions ratio. It consists of a two E-shaped soft iron yokes, placed opposite one another and with an air-gap between each of the three pairs of transverse limbs.

Excitation coils are placed on each half of the long arms of both yokes. They are connected, so their magnetic fluxes are in the same sense around the yokes circuit. Due to the symmetry of the circuit, without the specimen, there is no flux that crosses the centre air-gap. But, if a sample is introduced into one of the outer gaps, the symmetry is upset and a flux proportional to the value of the magnetization *M* of the specimen starts to cross the circuit across the central air-gap.

In order to measure the magnetization field inside the specimen (that should have the same value of the magnetic field outside the material) there were two sensors, one sensor is put in the middle gap, another just under the sample. This sensors are able to measure a deflection that is proportional to the gap flux: $H_{(cross\ \ arms)} \propto M_{sample}$ and hence to the magnetization of the sample.

The following equation shows how magnetization M is affected by the length L and the cross-section A of the specimen. C1 and C2 are constants which may be determined by calibrating the equipment. $M = \frac{C_1(1+\frac{C_2}{L})}{A}$

The calibration is very important for our measurements, indeed after each measure; it has to be check that without sample the system gives a horizontal line. Stablein-Steinitz measurement is designed for testing bulks samples. Therefore, starting from long bar specimens of different thickness, it was necessary to cut the specimens in some pieces of 20mm length, in order to create for each deformation rate a block sample.

For the as received material only one cut piece with area of 258.54mm^2 perpendicular to magnetic flux was used, while for 85% deformed, 6 pieces of steel were used to built a block, which the area in contact with the magnets was 243.64mm^2. The cross section of each block was calculated to make a comparison of each block with a reference block. This was possible because the calibration show a proportional relation between diameter of the specimen (or cross section) and the saturation magnetization value, and putting the value of the cross section in the Stablein software, knowing the specifications of the cylindrical aluminum reference sample, we achieve directly the real magnetization value of the sample.[7]

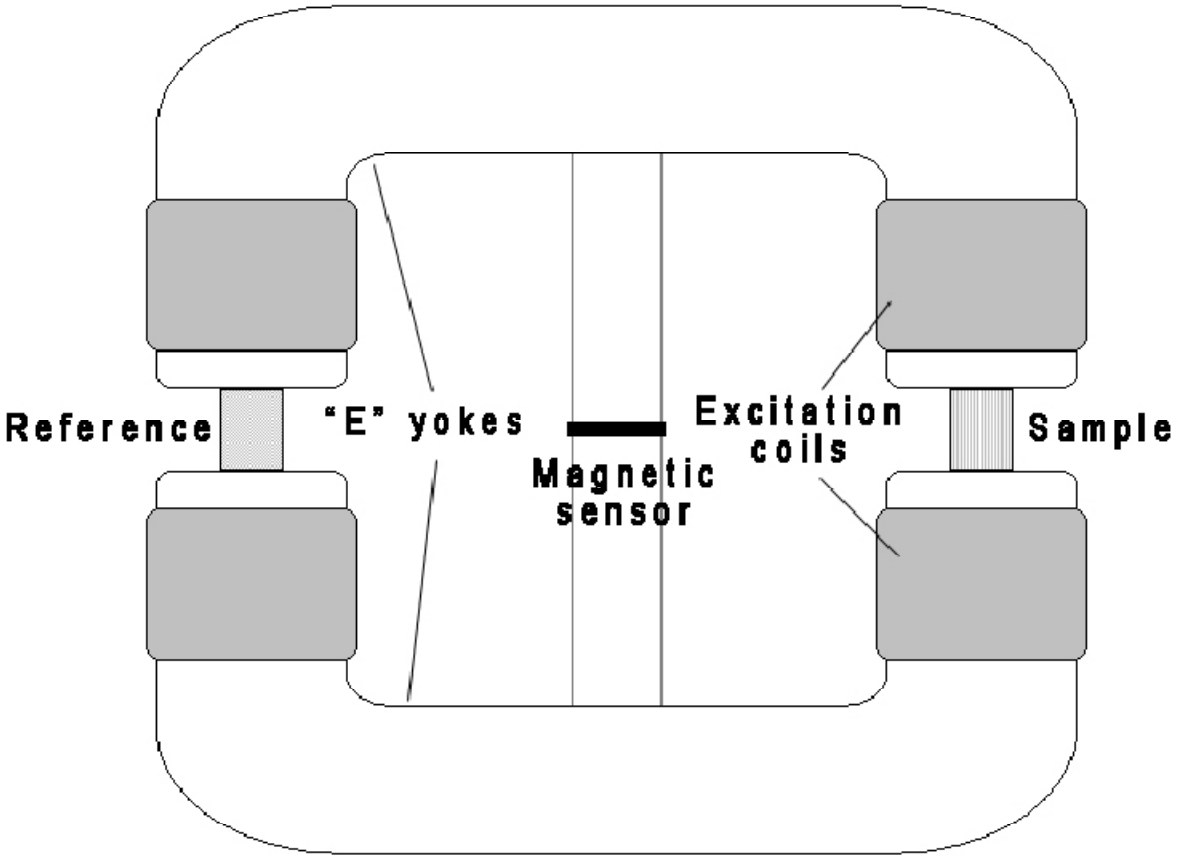

Figure 24 schematic of the Stablein-Steinitz instrument.

CHAPTER 4

Data analysis

A commercial 2507 SDSS was analyzed in the present investigation. The material was received as hot rolled bar of 12mm thickness in the solution annealed condition. The chemical composition is reported in the table below.

Element	C	Si	Mn	P	S	Cr	Ni	Mo	Cu	N
quantity	0.015	0.24	0.83	0.023	0.001	24.8	6.89	3.83	0.23	0.27

Seven samples were taken from this bar and cold rolled at 7 different thickness reduction: 0, 10 25, 35, 50, 65, 85%. A complete analysis were taken for all the cold rolled samples and then again after each heat treatment: one at 400°C for 2400s and in the second at 900C° for 2400s.

4.1 Optical metallographies

All the samples were investigated both on the transversal side (respect to cold rolling direction) both on the longitudinal side. Each sample was mounted in non conductive resin. For the optical metallographic analysis the Beraha etchant was used: 100ml H_2O, 20ml HCl, 1g Potassium metabisulfite; it etches ferrite making it darker than austenite that remains clear.

The hot rolled and solubilized material has the typical elongated grain structure, is possible to see white austenite grains in a matrix of dark ferrite. The cold rolling deformation has a relevant effect on grain's size and shape. Deformation effect is evident along longitudinal direction as stretching and thinning of austenitic and ferritic grains, and a packaging of them. The effect on the transversal direction is a crushing of austenitic and ferritic grains. As is possible to see, the reduction size of the grains in the most deformed sample is so great that only 50x of magnification is impossible to distinguish ferrite grains from austenite grains, moreover, the great elongation of grains lead to a chopping of austenite, it's a behavior emphasized with the increase in thickness reduction and it's possible to see this already on the sample at 10% thickness reduction.

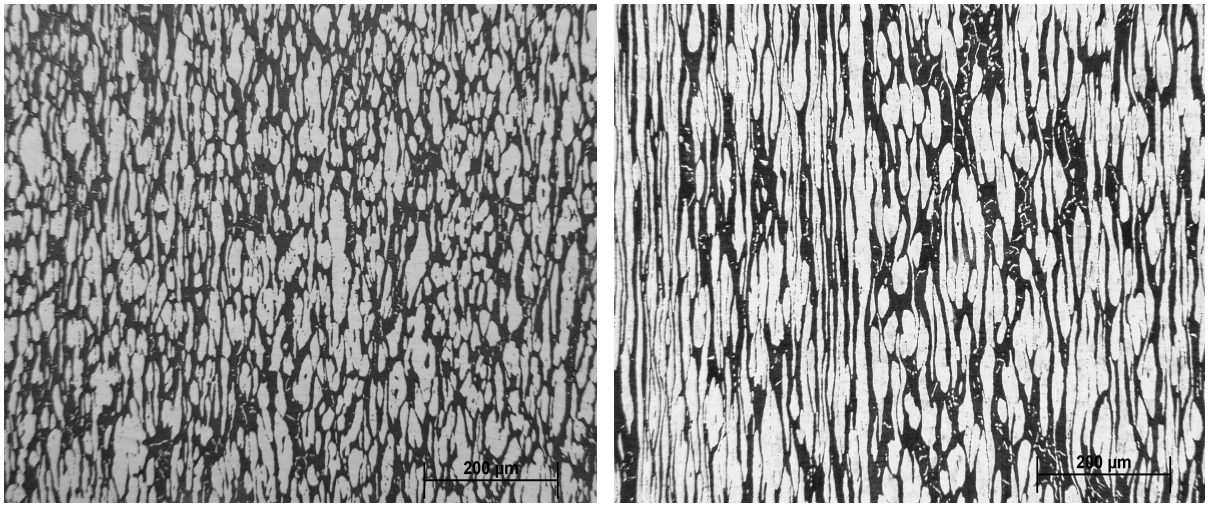

a) b)

Figure 1 (a) Base Material and (b) 10% reduction thicknes both at 100x of magnification.

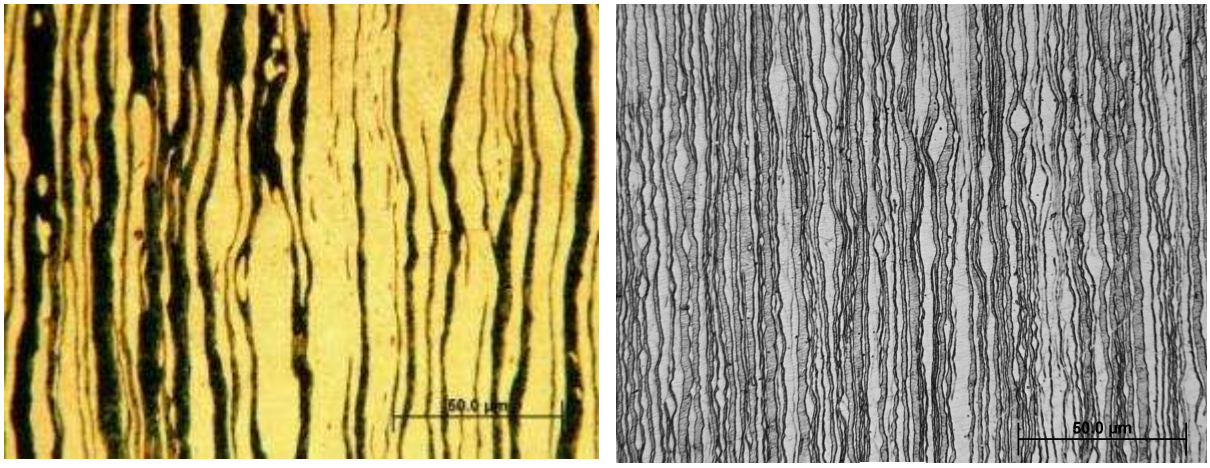

a) b)

Figure 2: 50% reduction thickness (a) and 85% red thickness (b) both at 500x, longitudinal section.

After 2400s at 400°C there is not considerable variation, and one can not appreciate any grain size variation; only in the first three samples is possible to see that on the ferrite grains there is a partition of the grains in smaller subgrains with formation of new boundaries. This behavior is shown also on a recent work about a 2101 lean duplex steel. However this behavior as shown later, no lead in differences in hardness. On the thickness reduction from 50% to 85% there is no partition of the ferrite grains. In no specimen were found other second phases.

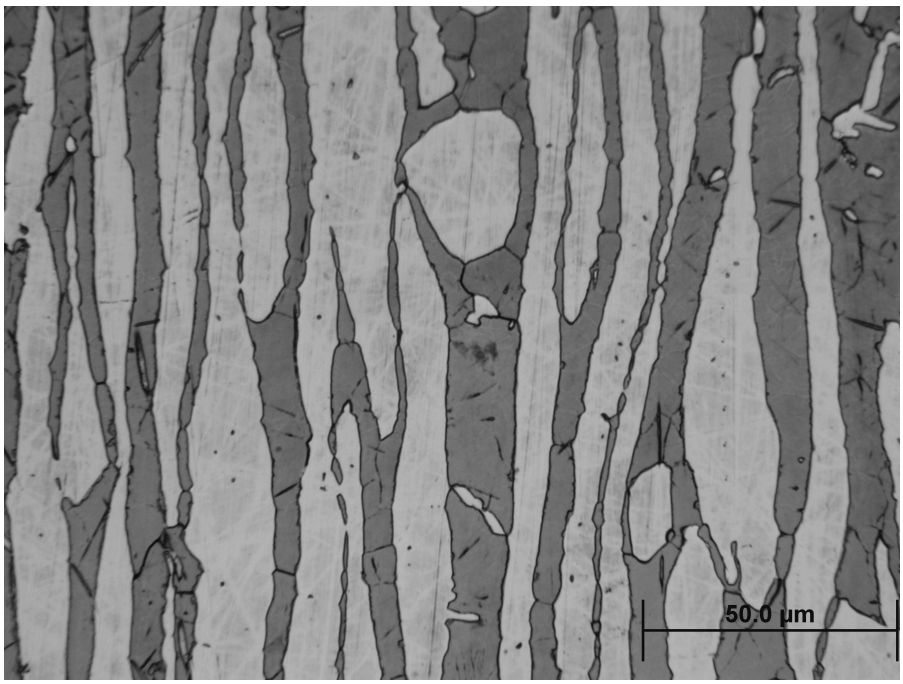

Figure 2 10% red thickness at 500x of magnification, longitudinal section, it is possible to see partition of ferrite grains after the treatment at 400°C.

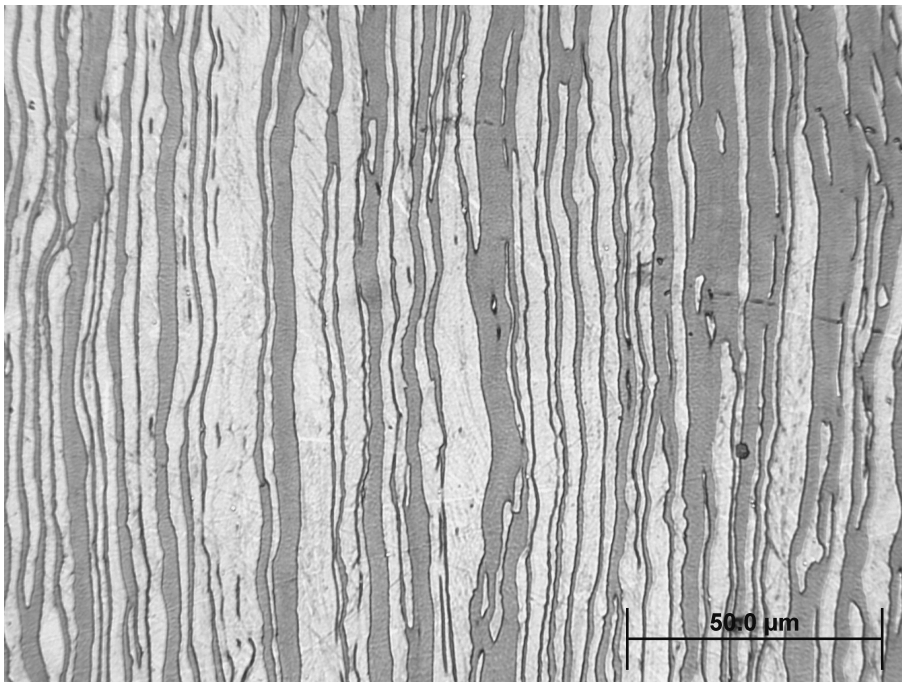

Figure 3 65% thickness reduction , is possible to appreciate the deformation bands on the austenite .

After 2400 s at 900C° there were some important differences. Is possible to appreciate the huge precipitation of sigma phase and secondary austenite. Sigma in the following picture is shown with white color. The sigma phase is mostly placed at the primitive ferrite/austenite interphase of the as-received material, but also some not negligible amount of sigma particles are observed into the austenitic grains, partitioning them. But this behavior is not shown in the base material and in the 10% thickness reduction; it starts to become important from the 25% thickness reduction up to the most deformed. In that case, the partition is strong, and also due to the very fine microstructure the distinction between different grains is now very difficult.

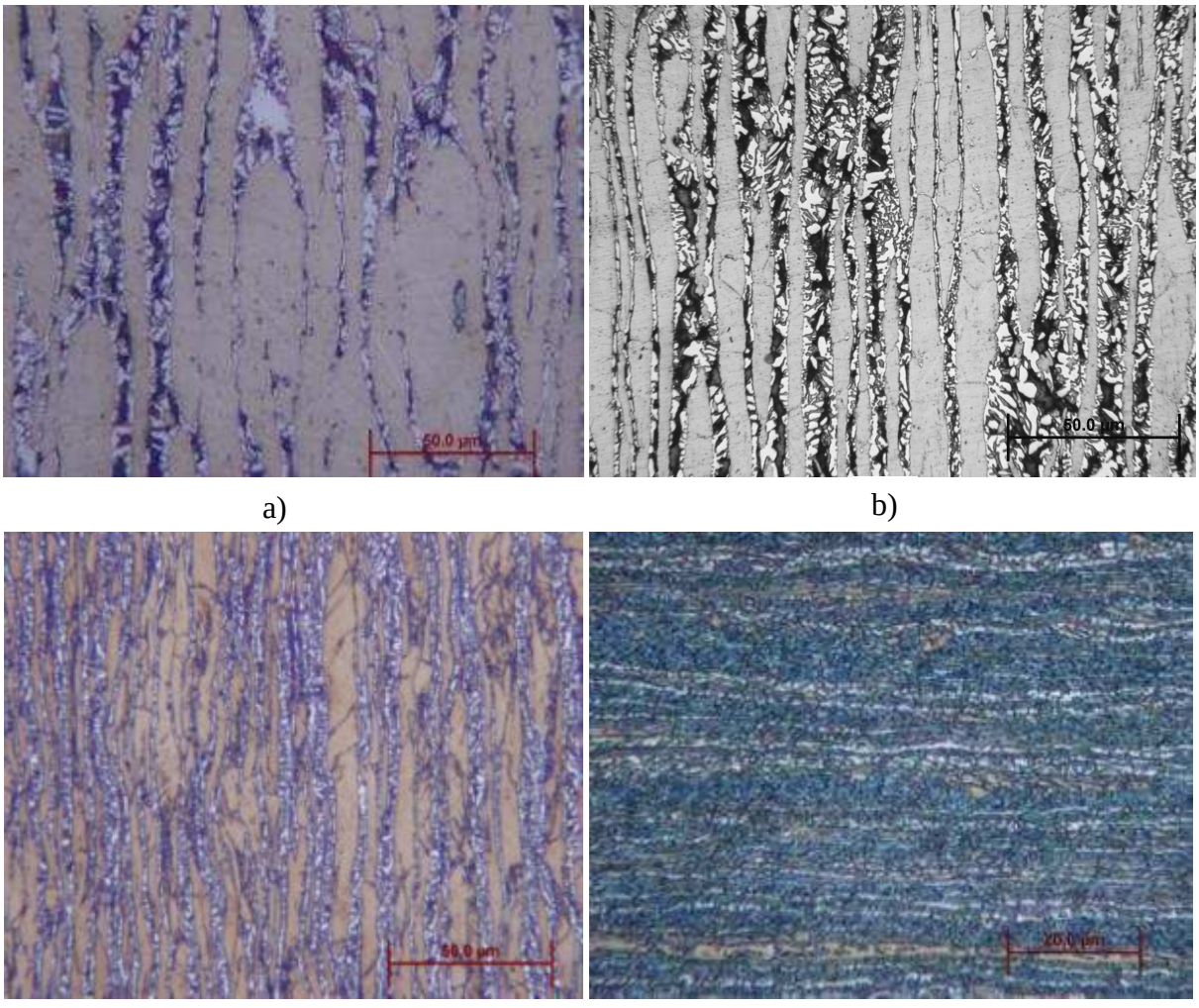

a) b)

c) d)

Figure 3 (a) base material at 500x magnification; (b) 25% thickness reduction at 500x magnification; (c) 50% thickness reduction at 500x magnification, the precipitation of sigma into the austenite is evident (d) 85% reduction thickness at 1000x magnification. All the pictures were taken after the treatment at 900°C, indeed there is a wide precipitation of sigma phase (in white).

4.1.1 Phase volume fraction

The micrographies of the non treated samples were investigated by an Image Analysis software. At beginning the pictures have to be digitalize by colouring different phases with different gray scale in order to sharpen the two phases. This step was done in order to measure the percentage of the 2 phases. After, there is the most important, and unfortunately the most operator dependant operation. This operation is the binaryzation and consists to assign to one phase or to the other a number of grey level. Ten measure for each sample were taken (5 for the longitudinal and 5 for the transversal direction). Anyway, the result of this analisys in the samples at cold rolled state seems according to the graph, that there is not variation of the δ/α ratio. Therefore, for all the 6 steps of deformation this ratio remains the same and so it is possible conclude that no new phase was found and there is no variation of the ratio, but this content will be better shown by magnetic tests.

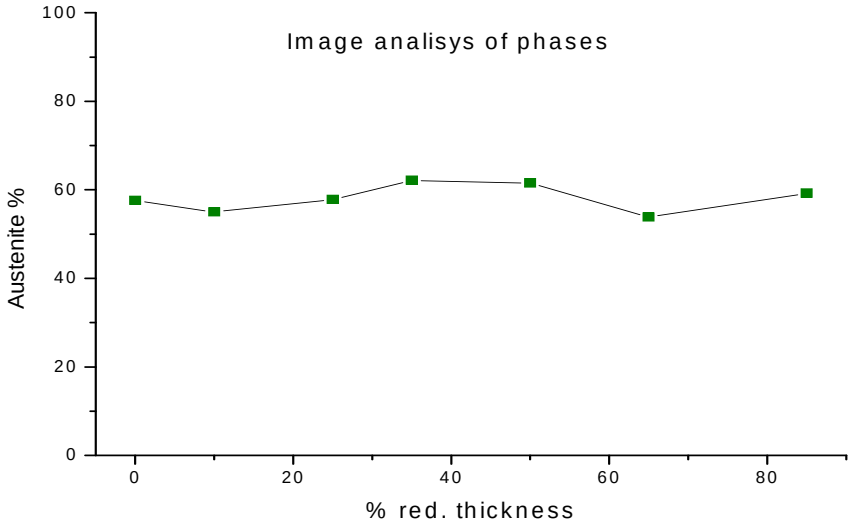

Figure 5 This graph show the image analysis results, on the non treated samples only.

4.2 SEM analysis

SEM microscope can perform analysis with more precision and accuracy respect OM, in BSE mode it can distinguish phases without the help of etching, while with the SE mode can show with extreme precision the morphology of the surface; but the main of the vantages is that the magnification can reach values that are absolutely forbidden with the OM. Austenite and ferrite are identified on the basis of chemical composition, with brighter areas corresponding to heavy atoms and darker areas where there are lighter atoms. The consequence is that austenite phase results brighter than ferrite phase and sigma phase results the brightest at all. Unfortunately, when it is present, is very difficult to distinguish the secondary austenite from the primary one because the composition is quite the same and a very small variation of the composition is not detectable.

Three samples were treated: the base material, the samples at 50% reduction thickness, and the sample at 85% reduction thickness.

The following pictures were taken with BSD and SE detectors.

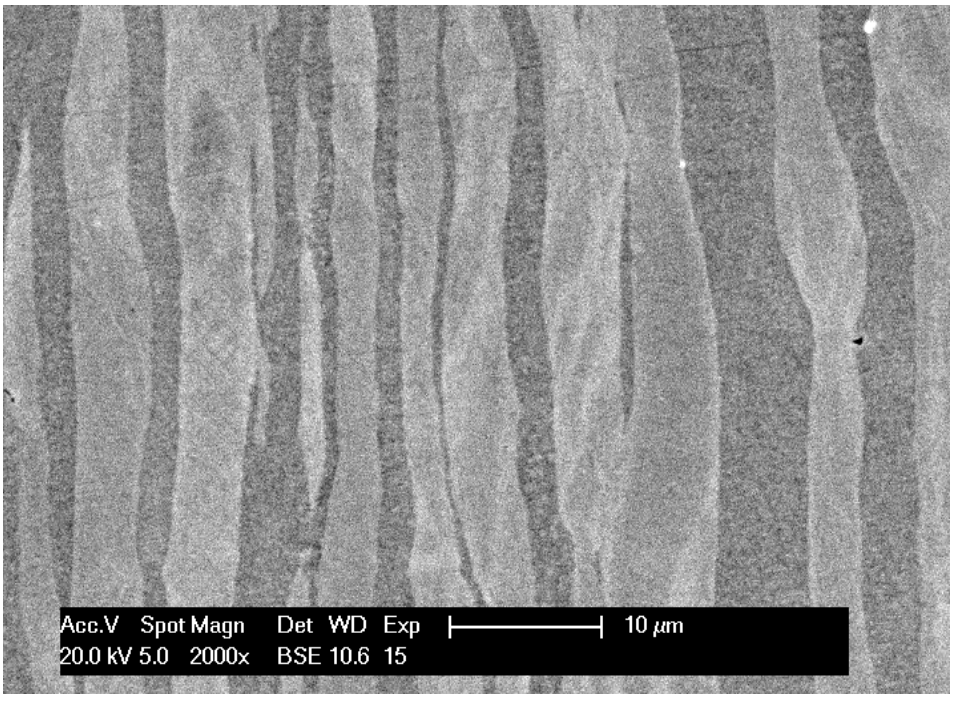

Figure 6 Deformation bands and twins in the austenite on the 50% thickness reduction. Is possible to see also a very bright dot, should be molybdenum carbide.

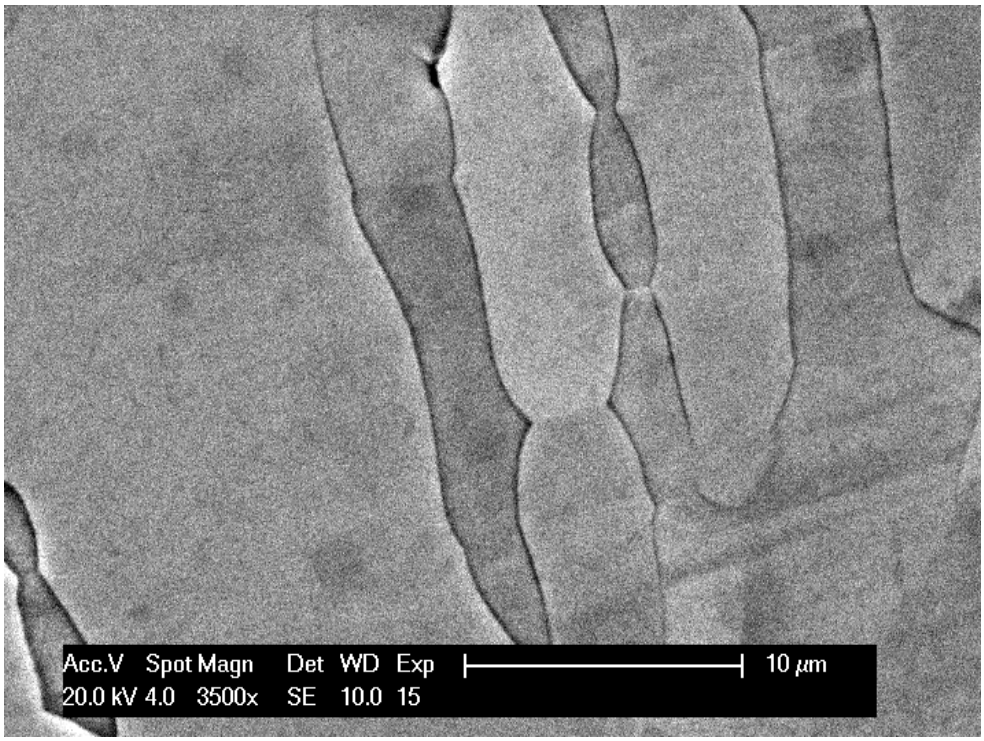

Figure 1 Ferrite grains partition after the treatment at 400°C. Base material, etched part.

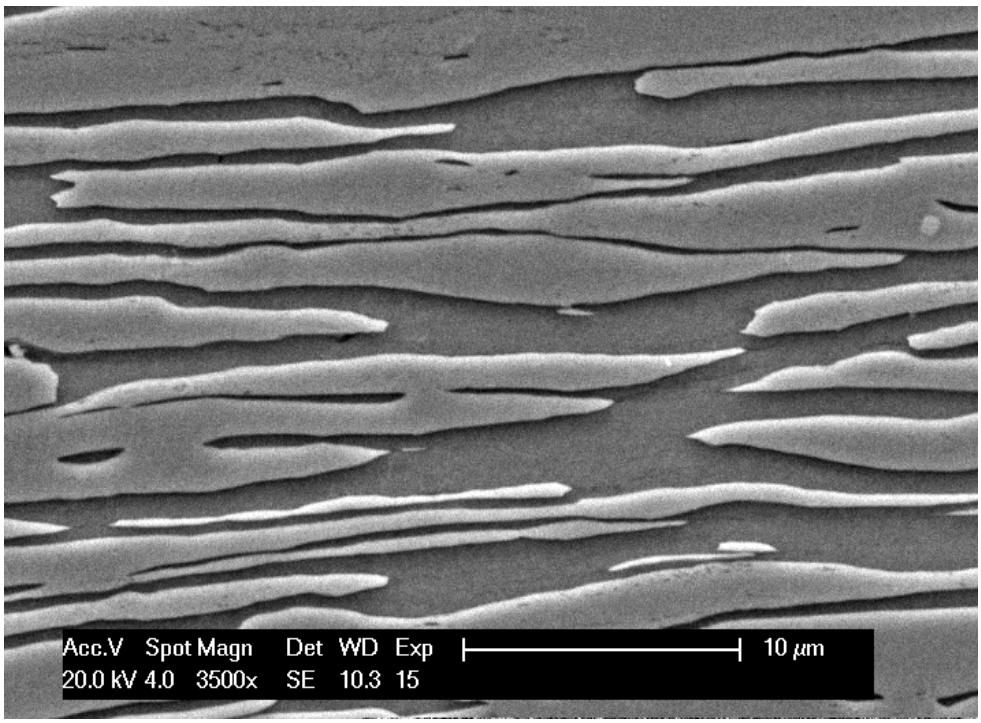

Figure 2 Grain elongation, sample deformed at 85% after 400°C

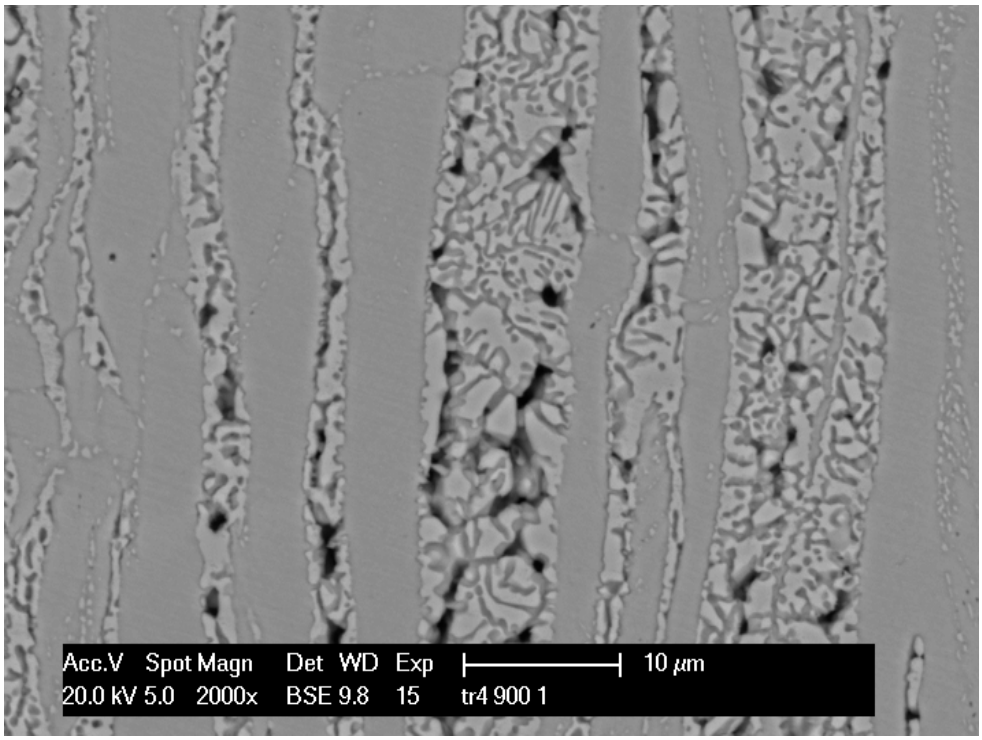

Figure 3 50% thickness reduction after 900°C treatment. It is possible to see the partition of the austenite grains by the sigma little precipitates, and the great decomposition of the ferrite.

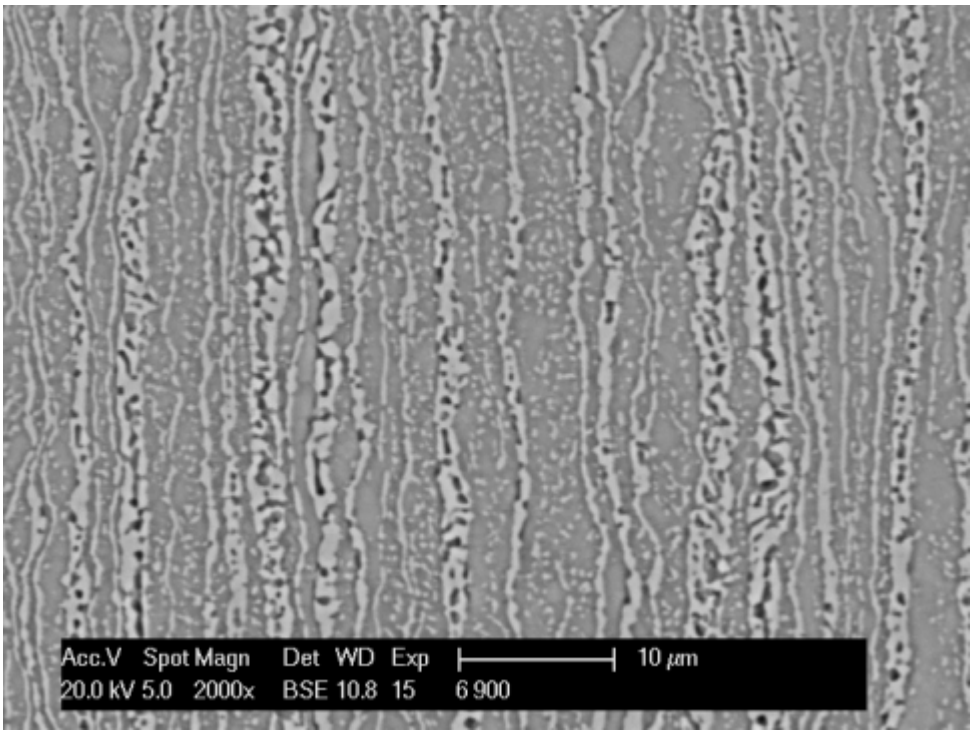

Figure 4 85% thickness reduction after the great decomposition of ferrite and the wide precipitation of sigma into the austenite grains.

4.2.1 EDS analysis

EDS permits the immediate identification of the elements present in the steel by a very rapid analysis of X-Rays emitted by it after the electron beam collision.
The phases analyzed with this technique were ferrite, austenite and sigma when showed, instead the base material and the samples at 50% and 85% of thickness reduction were analyzed before the treatments and after each treatment.
The following table shows the results of ferrite and austenite's composition on the samples before the treatments (only cold rolled state).

Sample	Base Mat.		50% thick. Red.		85% thick. Red.	
	γ	δ	γ	δ	γ	δ
Element	Wt%	Wt%	Wt%	Wt%	Wt%	Wt%
MoL,	3,01	5,09	2,84	4,37	2,68	4,17
CrK,	23,61	26,6	23,63	26,44	23,45	26,21
MnK,	1,09	0,91	1,72	1,79	1,54	1,86
FeK,	63,7	61,85	63,25	61,8	63,66	62,48
NiK,	8,42	5,56	8,57	5,6	8,67	5,29

Table 1 chemical analysis of ferrite and austenite in three samples.

The results show that nothing change in the composition of the ferrite and austenite for an increasing thickness reduction, sometimes there is a little variation like in the Molybdenum values but it's negligible. Cromium, Molybdenum and Silicon, ferritic elements, as expected are found in greater quantity in the ferrite, while an austenitic element as Nickel is contained more into the austenite. The values obtained are compatible with the composition stated by the supplier.
As shown in the previous pictures in the non treated but cold rolled samples there are some stripes and bands on the austenitic grains. It is well known that the BSD mode in the SEM give a good contrast if there are phases which contain atoms with different atomic weight. So, a brighter area correspond to heavier atoms respect to the darker, that should contain lighter atoms. The analysis in this austenite areas were carried out twice time both in the 50% reduction thickness both in the most deformed, but no valuable differences were found; the results are in the following table for the sample at 50% thickness reduction.

	γ dark	γ brigth
Element	Wt%	Wt%
MoL,	2,68	2,84
CrK,	23,45	23,63
MnK,	1,54	1,72
FeK,	63,66	63,25
NiK,	8,67	8,57

Table 2 No difference in composition was found between the bright and dark areas into the same austenite grain.

Is possible to find, only on the base material, some very small precipitates, very bright. At the analysis they show high content of Mo, so it is supposed to be molybdenum carbide and they are very bright because they're non conductive and remain an electrical charge on the surface of the carbide. Anyway in the followings analysis no more precipitate like this was found.

After the treatment at 400°C for 40 min, no difference in composition of ferrite and austenite was found in the three samples. Austenite and ferrite maintain the same composition in all the analyzed samples and the results are the same of the non treated samples, so, the previous table can perfectly represent also the treated samples. However, the following one, referred to the most deformed sample, can better describe the situation.

	No treated		Treated for 40 min @ 400°C	
	γ	δ	γ	δ
Element	Wt%	Wt%	Wt%	Wt%
MoL,	2,91	5,23	2,68	4,17
CrK	22,96	25,87	23,45	26,21
MnK	0,76	0,82	1,54	1,86
FeK	64,23	62,13	63,66	62,48
NiK	8,54	5,36	8,67	5,29

Table 1 Composition of the sample deformed at 85%.

In the samples treated at 900°C for 40min, there was a big amount of ferrite decomposition, therefore, the analysis of the ferrite in these samples was very difficult, because its small quantity and dimension. So, the spot analysis in this very little area, can lead not negligible mistakes because an eventual chemical analysis would be affected from the

surrounding. For this reason is preferable show only a comparison of the austenite, where the analysis was carried out easily.

	base mat	50% thick. Red.	85% thick. Red.
	γ	Γ	γ
Element	Wt%	Wt%	Wt%
MoL,	2,81	3,65	4,03
CrK,	24,95	24,47	24,62
FeK,	63,61	63,09	61,59
NiK,	8,64	8,79	8,01

Table 2: differences in composition between austenite phase about three different samples after the treatment at 900°C. The molybdenum seems to increase with the deformation rate.

The first conclusion is that the treatment in the base material has not affected the classical composition of the austenite despite the abundant precipitation of sigma phase. The situation is different for the deformed samples, especially the last, where it is possible to see that (from several measures) the Mo content increase.
Anyway the ferrite analyzed on the base material show the classical composition. The sigma phase show the classical high content of Cr and Mo.

	σ phase
Element	Wt%
MoL,	7,39
CrK,	29,6
FeK,	58,44
NiK,	4,57

Table 3 Average composition of the sigma phase checked in the samples.

Is well known that on this kind of steel at high temperature the eutectic decomposition of the ferrite in sigma phase and secondary austenite occurs; but it is very difficult to discriminate this secondary austenite from the original one, because the composition should be the same. It was tried to check some differences in austenite composition but how expected no differences were found (between checks in the same sample.)

4.2.2 EBSD investigation

This equipment can give us a lot of useful information, for example the phase ratio and the crystallographic orientation of each phase. Unfortunately this technique is strongly dependant from the surface's condition: morphology, roughness and stress state. An optimal surface has to be perfectly polished (also up to 0.01µm) and without stresses, can help also a little bit of etch. Indeed with the non treated samples only the base material was analyzed very well because on the 4 and 6 samples (not analyzed at all) the stress state was too high and the kikuchi lines were difficult to detect giving an IQ very low. Only on the samples treated at 900°C, despite the decreasing of IQ up to the most deformed, the samples 4 and 6 were analyzed.

The analysis of the phase ratio is easy with EBSD, the system takes a picture, this can be "cleaned" by choosing the minimum grain size to detect; the phase map just created gives immediately the information on the phase ratio. Unfortunately the cleaning step is strongly operator dependant, if the grains are big the is no problem but if there is very fine structure the probability to miss some information and to mistakes starts to be considerable.

Magnetic tests show that the phase ratio is about the same in all the samples, also after treatment at 400°C. The EBSD confirm this, the results are little different but this is due to the fact that the analysis is about some surface picture and not about the bulk material. The following table are about pictures at magnification of 500, 1000 and 1500x.

	No treated		Treated at 400°C		Treated at 900°C	
	δ	Γ	δ	γ	δ	γ
BM	0,467	0,533	0,487	0,5085	0,0585	0,8275
50% thick red.	0,573333	0,426667	0,533	0,466	0,035	0,704
85% thick. Red.					0,025	0,851

Table 3 comparison of the content of γ and δ between samples after the treatment at 900°C.The last row is partially empty because there are not measurable ferrite in the first two samples

The phase maps related to the analysis, are in the following page, with special attention to the phase maps after the last treatment.

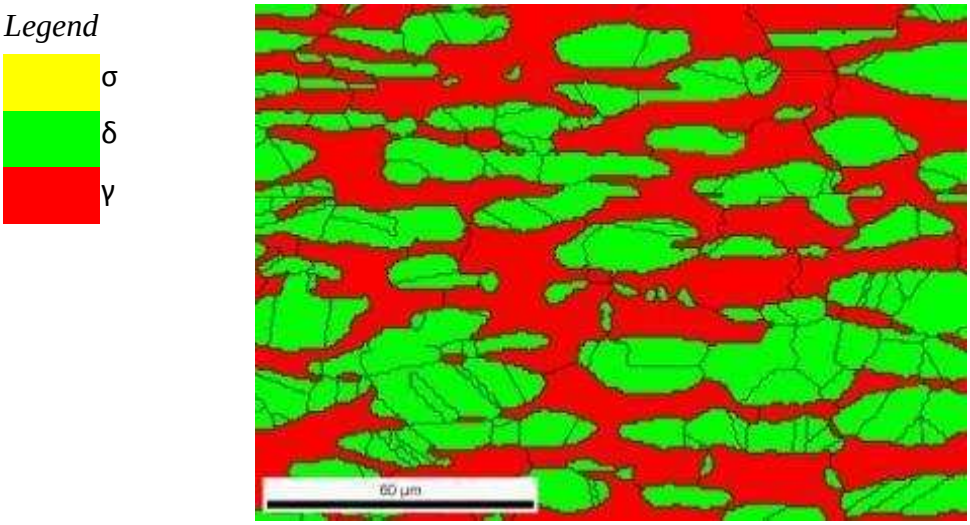

Figure 5 : base material before each treatment.

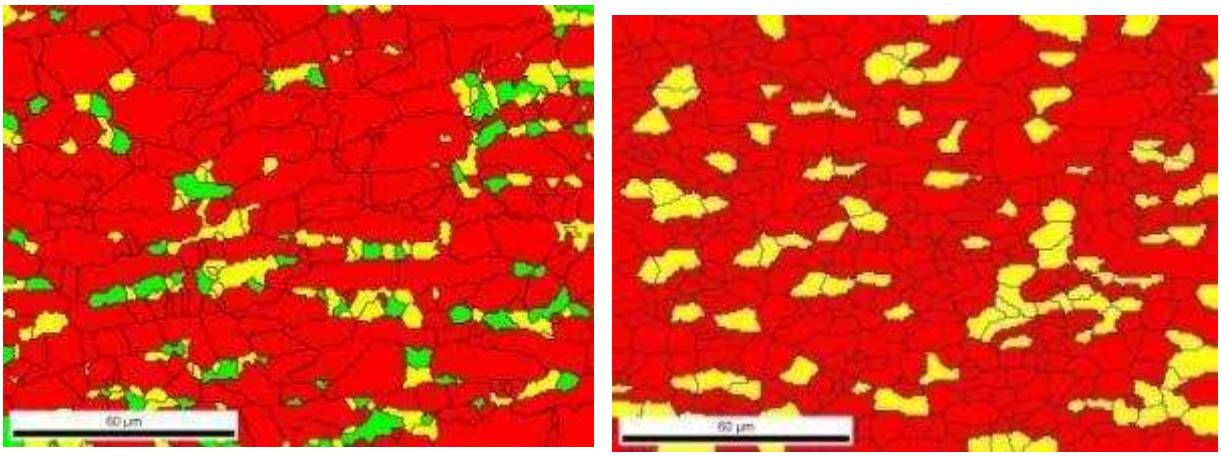

Figure 6 On the left is shown the BM, on the right the 50% thickness reduction; both after the treatment at 900°C

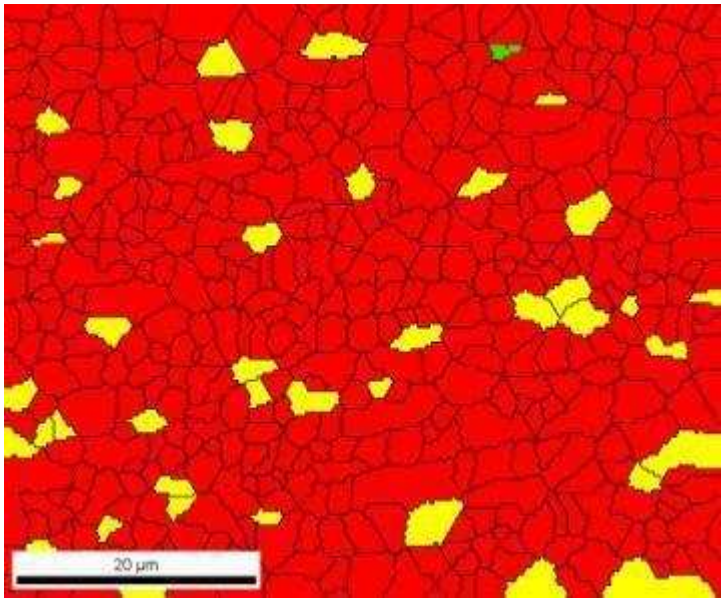

Figure 7 85% thickness reduction after the treatment at 900°C.

All the previous pictures are been taken with a minimum grain size of 10μm and the boundary are drawn with minimum misorientation of 15°. The great precipitation of sigma phase is evident, but not the same quantity for all the samples. The following table shows the trend of precipitation of sigma with the deformation rate; it seems that is favorite the formation of secondary austenite instead of sigma is formed.

	BM			4th(50%)		6th(85%)	
Sigma %	16.1	10.7	11.8	27.5	24.5	8	13
Aust %	82.9	82.6	77.9	69.5	71.3	91	85.9

Table 5 Percents of sigma phase and austenite in the three samples, it seems the sigma phase decrease in content from the 50% to the 85%thickness reduction.

The χ phase is difficult to find, it was not detected because it is cubic as the ferrite and the parameters setted on the ebsd leads the software to a confusion between χ and ferrite showing sometimes big island of χ phase that of course was not true.

In the followings pictures there are a grey scale map of the pattern quality related to the correspondent phase map: lighter pixels correspond to areas with a sharp and clear pattern, while darker pixels are related to regions of poor pattern quality due to high intensity of defects (such as grain boundary regions, deformed material, submicrometer structures).

The samples treated show interestingly that new formed phases present generally a low quality pattern than pre existing phases. This behavior is especially showed with the σ phase as clearly visible in the figure.

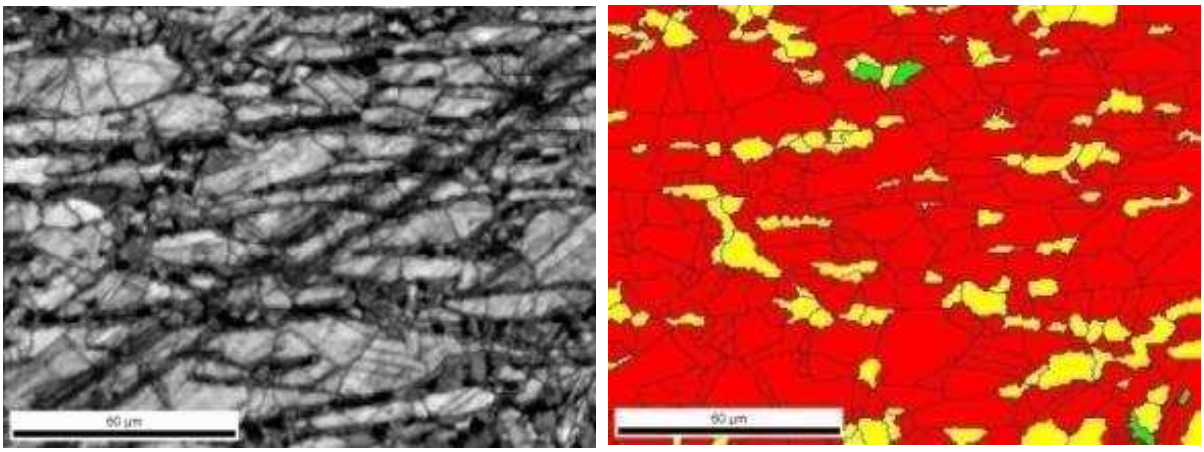

Figure 8: IQ map versus Phase map. On the areas of nucleation of sigma phase the pixels are darker, it means there was a stress rise.

The following picture present some inverse pole figures about ferrite, austenite and sigma phase. All the orientations are ND based.
From EBSD results for these samples it is possible to say that crystallographic texture of the austenite is {hkl} <111>.

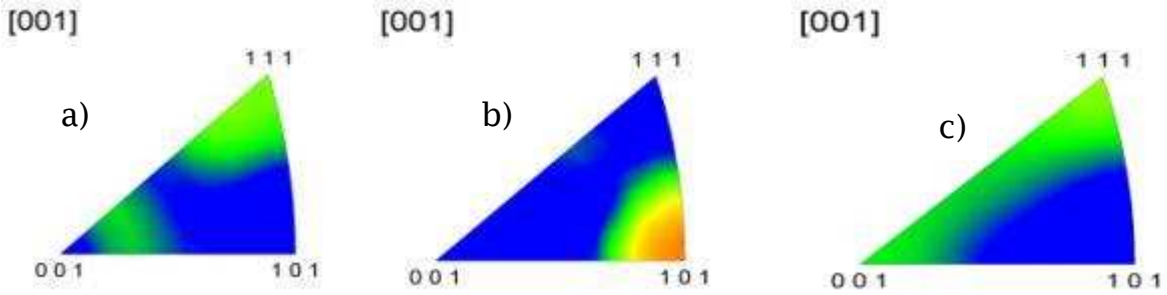

Figure 9 IPF of the following phases:(a) austenite orientation on the base material; (b)Ferrite orientation on the 50% reduction thickness (c) austenite orientation after precipitation of sigma on the base material.

The orientation of the austenite and ferrite became less spread, it concentrate with the deformation, and is possible to see this by the change from green to orange of the colour in the IPF.
After the last treatment, with the formation of new austenite and sigma phase, the overall orientation of austenite change a little spreading from 111 to 001 direction (figure c). The IPF of sigma phase are in the following pictures.

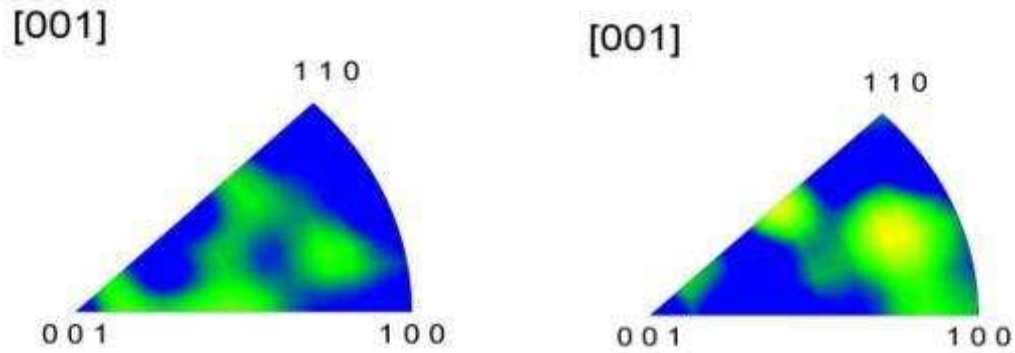

Figure 10: IPF of the sigma phase. Left 50% thickness reduction; right, base material.

4.3 Micro-hardness test

In the hardness test each sample was indented 5 times in the longitudinal side and in the transversal side, in total 10 measures for each sample, for each sample the average measure is shown. The device was setted for a Vickers test with 200g of load and 5sec indentation time.

The mechanical hardness increases rapidly with the first step of thickness reduction. The dislocations start to move and to increase their amount due to the energy supplied by the deformation. Then, they start to interfere with each other, stacking and blocking themselves, and the mechanical hardness increases. Unfortunately this kind of measure is only a surface test and didn't give us information about the bulk; this is the statement because the cohercivity doesn't follow very well the hardness increase.

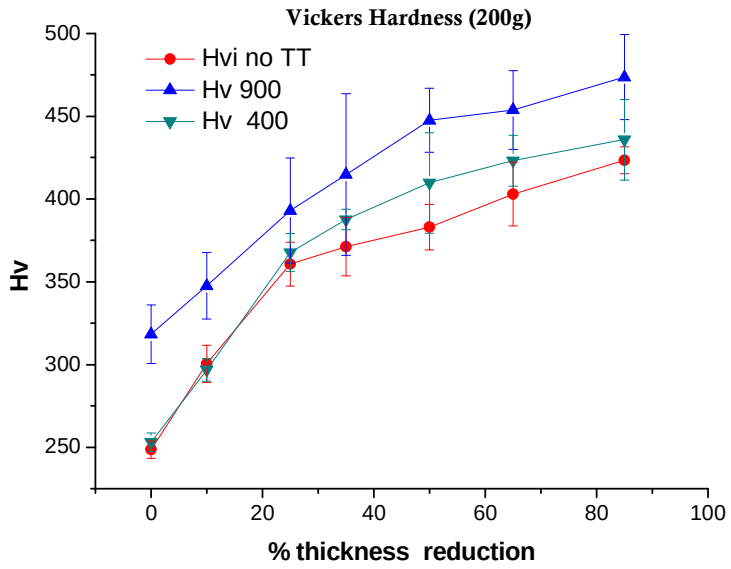

Figure 8: Vickers hardness of the samples before and after the treatments.

As shown, after the first treatment the hardness is exactly the same of the non treated for all the samples except for the last four, and the increasing of hardness follow the same conduct. Anyway the SEM shows that there is any hardening precipitation, and the hardness as known is a measure strongly dependant on the operator so some errors or strange result are expected.

After the second heat treatment it is possible to see that the hardness is quite increased, and also the way of increasing is not the same of the

previous two group of measures. This is due obviously to the high amount of sigma phase precipitated. The sigma phase is hard and brittle ad growing into the matrix substituting with secondary austenite the decomposed ferrite, give raise a stress state in all the steel.

4.4 Ferrite tester

The samples used for this test was the same for the Stablein test. The measures were taken both on the face both on the sides (always five per side) with different polishing grades in order to evaluate the influence of this on the measured values. The measurements on the sides of the most deformed sample were not taken because of the difficulty for the operator and the instrument to measure a thickness of only 1.94mm with a probe of 1cm of diameter.

Measuring the ferrite quantity the following behavior was observed: the average value of the values measured on the face was always lower than the values measured on the center of the side. It means that the ferrite content increase from the surface (the cold rolled surface touched by the cylinder) towards the center, therefore, is not possible consider valid the surface value for all the bulk, anyway a comparison of the surface value for all the samples is showed in the graph on the conclusion paragraph. To give an idea of the difference, the percent of ferrite in three different zone was calculated: the face and two time the side polished at 2 different mesh.

Area	*side pol.80*	*side pol.320*	*face (as rolled)*
Ferrite %	4,56	3,72	1,16

Table 4 Differences in the ferrite content measured between the face and the sides polished with different mesh.

Each data of the graph is an average of 5 measures of the same zone. As shown, in the side there is always a value of ferrite very high respect to the value of the face.
However, in the samples treated at 900°C the Ferrite Tester shows a decreasing value (in the face) that is confirmed by the magnetic tests.

4.5 AC magnetization curves test

With AC tests it is possible to obtain many information from the material, unfortunately the excitation field supplied by AC is not enough to saturate this kind of material, and this is generally valid for each ferromagnetic material, therefore, this device can only draws internal hysteresis loops (not the saturation one) and internal firsts magnetization curves.
Saturation field or magnetization, permeability and coercivity, influence the hysteresis loop shape. But if the first one is determined only by the composition of the material (is not structure sensitive, it depends only on the magnitude of the atomic magnet moment and on the number of the atoms per unit volume), permeability and coercivity are sensitive also to structural variables (they are structure sensitive) apart from the composition. If the domains are free to move when an external magnetic field is applied, the coercive force value will be low, while, the presence of structural defects (e. g. particle of nonferromagnetic phases or dislocations) limit the domain walls motion, increasing the coercivity. As we know also the permeability is influenced by the internal structure and stresses, indeed, the peak of $\mu_r max$ move towards higher values of magnetic applied field with the deformation rate.
Coercivity and remanence increase their value due to high thickness reduction. The B_{max} (the maximum magnetization value measured) remains still around a value (about 0.57 T) increasing the plastic deformation, so the only effect is an enlargement of the hysteresis loops as expected.

The excitation field of the AC test is relatively small than the field required to reach the saturation, therefore, virtually, the magnetization value (that is not the magnetization saturation value, because the domain are not all oriented) is little higher for the as received material than the other deformation states, because it is easier to magnetize a stress-free material, and anyway we are still on the internal loops; but the most evident result is the shape of this hysteresis loops, with a big enlargement after the sample with 10% reduction thickness. Conseguently, the $\mu_r$max (that shows the tendency of a material to be magnetized) decreases for high deformed materials. It was calculated from AC data and not from Stablein data because the AC instrument can give a better first magnetization curve. As is possible to see, for a fixed excitation field, the as received material is more easier than a deformed material to be magnetized.

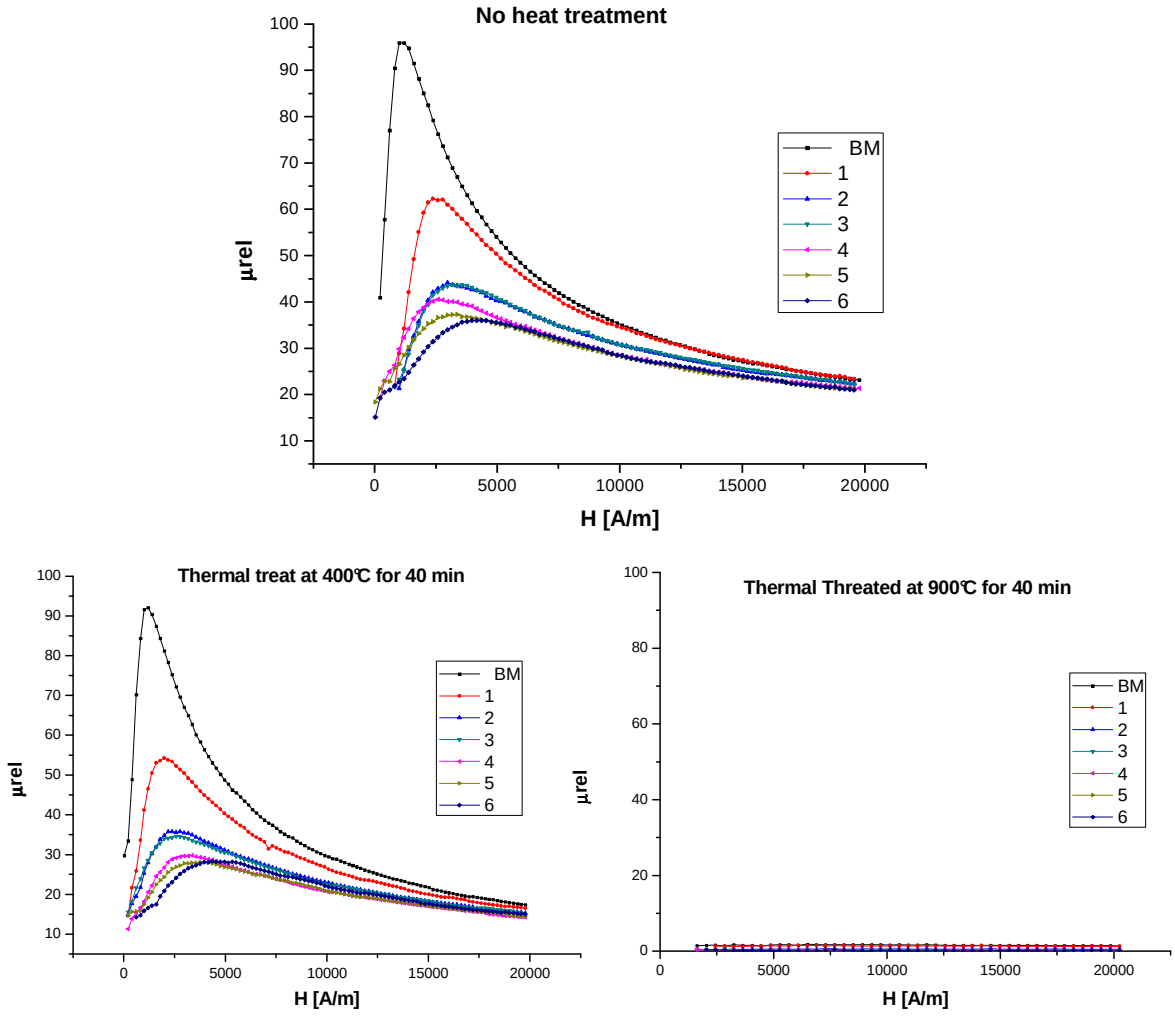

Figure 9:relative permeability before and after each treatment. The AC test failed to magnetize the very low amount of ferrite remained after the treatment at 900° for 40 minutes.

The magnetic hardening and hysteresis loop enlargement are related to the freedom of movement of magnetic domains. 85% deformed material for example, has magnetic domain boundaries more pinned than others deformation states, therefore this causes an increase in the energy lost during magnetization process in the form of a kind of internal friction. So, it is possible to see the relative permeability decrease and the peak move towards high excitation fields.

About the permeability, after the first treatment it is possible to say that, as expected, nothing changes and the values are quite the same of the non treated samples. For the treated at 900°C the little excitation field of this AC device is not enough to magnetize the very little ferromagnetic phase remained, so the calculation of the permeability give all values around the zero.

4.6 Förster magnetometer

Forster test is a DC measurement designed only for accurate coercivity measurement. It is able to supply an high excitation field (about 1000A/cm). This kind of test was exclusively projected to measure real coercivity from saturation curves. It is an open circuit magnetic equipment, so the H_{IN} that affects the specimen is smaller than the H_{OUT} supplied; but, being D of the order of 0.01 the H_{out} is enough to saturate the material according to the empirical formula that if $H_{supplied} > 5H_c$ the material is saturated.

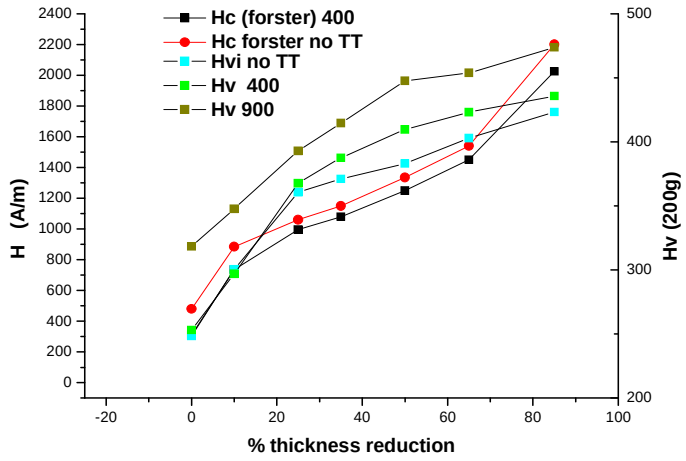

Figure 8:Comparison between the measured hardness and the coercivity by Foster.

The graph in the previous figure shows the correlation between the hardness and the coercivity measured by Fosters instrument. Coercive values increases for high thickness reductions: the number of pinned dislocations increase for high deformation rates, and this increases the hardening therefore the domain wall movement is limited respect to the beginning and the coercivity increase.

The coercivity curve doesn't approach very well to the Vickers hardness curve; this is due mainly to the fact that the two measures follow different ways, one is a surface measurement, the other is a bulk measurement. In the first samples (low thickness reduction) mainly the surface of the material is interested by the deformation, while the bulk remains like the initial state, and until the sample rolled at 10% the two curves approaches each other. Being the coercivity a bulk measurement it cannot give the same value measured in the surface when the deformation rate start to be important. And a confirm of this seems to be (because at high deformation rate the coercivity approach very well the hardness) that when the deformation rate is very high and all the material is involved, the surface measurement is similar to the values eventually measured at the center because the state of the material now is similar both in the surface both in the center.

After the treatment at 400°C it is possible to see that the hardness values are little greater than the respective value before the treatment, this despite no variations (any precipitation of other phases, any trasformations etc...) were found both at OM both at SEM.

It was impossible to carry out tests with this device for the samples after the treatment at 900°C, this because there was not enough ferromagnetic phase to magnetize (except the first two sample) and the values showed was very low and the trend was decreasing instead of increasing.

4.7 Stäblein Steinitz test

Stablein-Steinitz measurement is a closed loop DC measurement which is based on a symmetrical magnetic bridge yoke. It is able to supply an excitation field over 200˙000A/m, greater than AC measurement test.
It is enough to saturate an hard magnetic material such as this SDSS.
About the first magnetization curves, the little shift that can be noticed is due only to the instrument (positioning of sample, noise etc...). So, this confirm again that in this steel there is no differences in the amount of ferromagnetic phase after several degrees of cold rolling. The same conclusion can be drawn watching the hysteresis loops that are exactly the same for each sample, again, all the sample reach the same value of magnetization and the little shift are only due to the device problem.

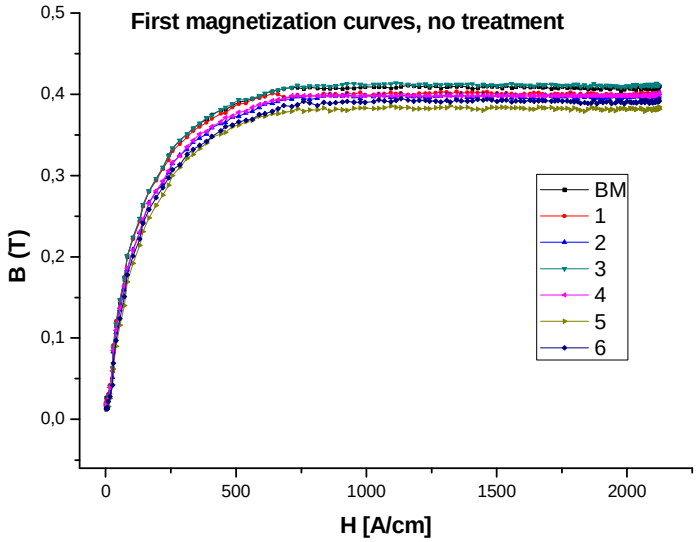

Figure 8:First magnetization curves of the samples at only cold rolled state: there no detection of further ferromagnetic phase..

Anyway, the curves drawn by the device are not horizontal for high excitation fields, therefore it is impossible to derive the saturation magnetization value from these, because the magnetic induction could increase linearly to the infinite for higher and higher excitation fields. This behavior is due to an error of the instrument that, also without sample mounted, instead of giving an horizontal line (B=0) it gives a line constant increasing with slope of the order of $1*10^{-5}$, and this slope is

recognized (and has the same value) in all the first magnetization curves, therefore by subtracting a line with this slope from the first magnetization curves we can obtain the magnetization saturation value.
About the treatment at 400°C, is possible to say again that nothing changes between the samples treated and not treated, also the first magnetization curves are identical.
After the treatment at 900°C the situation change radically; the ferrite decomposes and leads to samples very poor of ferromagnetic phase. The graph about the first magnetization curves shows detectable amount only on the first 2 samples. It is evident that the high deformed samples decomposed their ferrite faster than the less deformed samples.

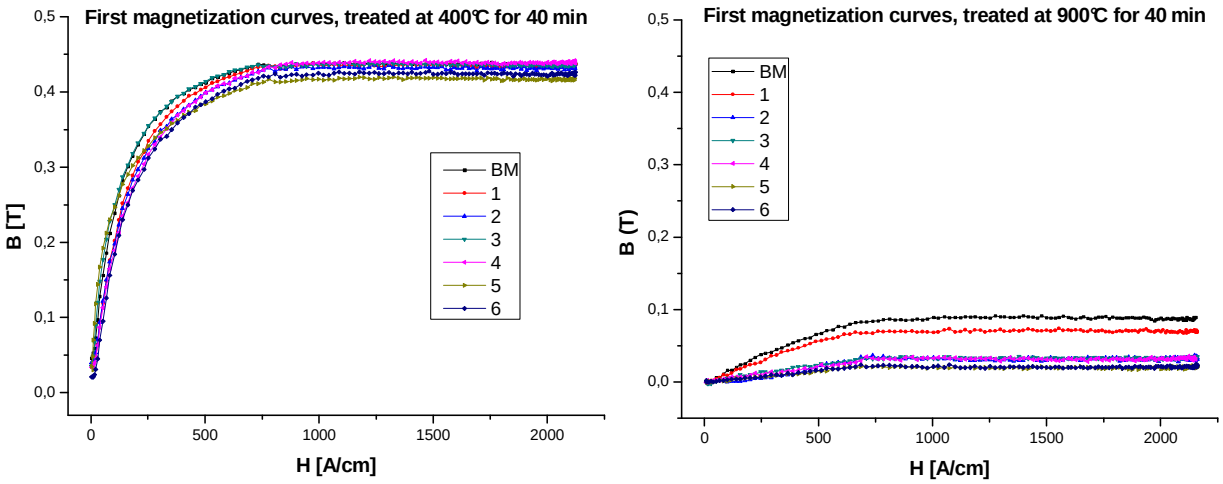

Figure 8: First magnetization curves of the samples after the treatments. The device detect appreciable ferromagnetic phase only on the first two samples.

4.8 X Ray diffraction

After polishing the samples, the XRD was carry out in the directions of rolling only in the usual 3 of the non treated samples. Radiation Cr Kα (2,2897 Å) was used for these measurements.

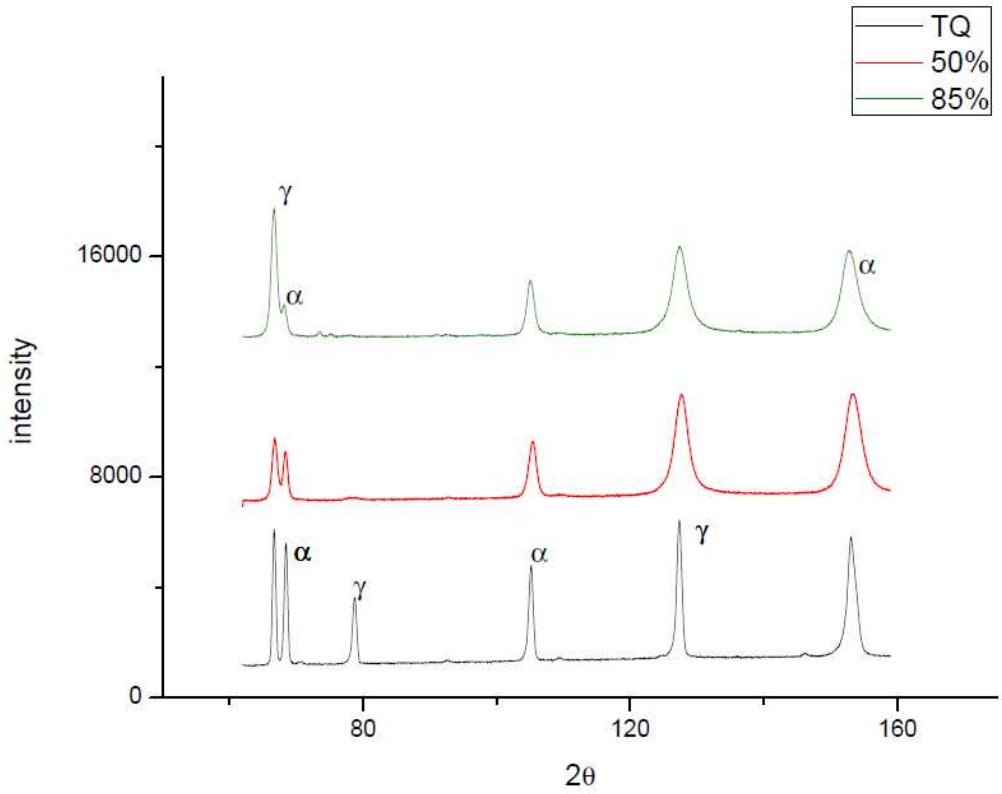

Figure 11 XRD patterns of the three samples analyzed. The peaks have not comprensible behavior

It is possible to see the strange trend of the first peak of austenite that decreases for the sample rolled at 50% and then increases again for a further rolling. This is a very strange behavior and have no theoretically explanation. Is also strange that the peak of ferrite decreases with the increasing in deformation. Of course, this behaviors was not confirmed at all by the magnetic tests that show a quite constant content of ferrite and austenite in all the samples.

A statement of this could be that being the xrd a surface measurement, in the path of the beam there was not a lot of austenite in the 50% deformed samples, but this is not enough to say that the austenite is decreased in all the sample.

Not less important is the fact that, the XRD is a technique based on the distance *d* between the crystal planes and everyone know how distorted is the lattice of the crystals especially after a hard plastic deformation. This is surely a thing that lead the instrument to commit mistake.

4.9 Comparisons and correlation

4.2.2 Martensite transformation and magnetic tests results.

Starting the investigation by the calculation of the forecast index Md and SFE respectively of -203.67°C and 45.35, the eventually transformation of the austenite to martensite would be surprising. Therefore despite the low nickel content on the austenite (circa 8%) it does not transform by deformation in martensite, although for example in the 304/8 with 8% of Ni the transformation of austenite in martensite occurs widely: more than 50% with only 60% of thickness reduction [30]. This, of course is a different steel , and one of the main difference is the content of nitrogen and molybdenum. Indeed in the 2507 sdss under investigation there is a strong role played by Nitrogen, that its already well known to improve the corrosion and wear resistance.

Nitrogen is a very small atom that can reach the interstitial area of the iron lattice and contributes to block it making it more stable, indeed is a stabilizer of austenite that is FCC, and can contain in the central space an atom of nitrogen. During the deformation many vacancies were formed and nitrogen can occupy many of these, blocking the dislocations and acting like a source for these . Previous works on a lean duplex 2101 and on a SAF 2205 show that was found martensite transformation, but here the nitrogen (and the molybdenum) content was very low respect to a 2507 sdss [7][10]. Concluding, it is possible to say, according to the results that the forecasts of Md and SFE about the transformation of austenite in

martensite was respected; indeed the magnetic tests revealed no variation of ferromagnetic phase content.

The following graph is about the calculation of the Non Ferromagnetic Phases (NFP), that is an index widely used in the scientific articles. This value can be determined easily by relating the value of the magnetic saturation of the specimen (*Jm)* to the magnetic saturation of a fully ferritic reference sample J_s^{ref} = 128 [Am²/kg] (value found in an article about the 2507 [24]) using:

$$NFP = \frac{Js^{ref} - Jm}{Js^{ref}} * 100\% \text{ [27]}.$$

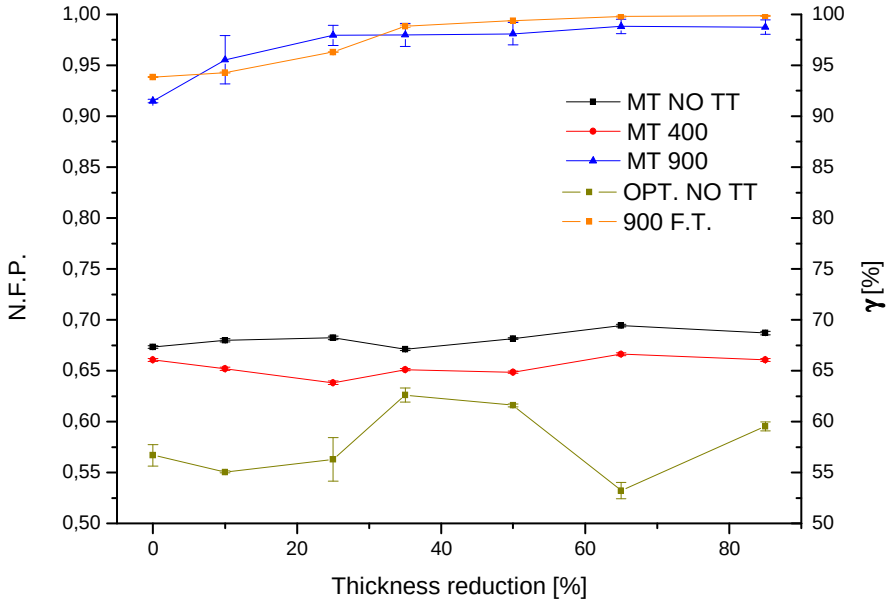

Figure 8: NFP and austenite content on the samples after and before the treatments.

The calculation of this parameter for the only cold rolled samples from the magnetic tests, shows that is quite in agree with the result of the optical investigation. Being the optical microscope analysis only a surface investigation it is considered not precise as the magnetic tests, these show a slightly more content of austenite (and a more stable trend) respect the results of the optical test.

In a recent work about the super duplex steels, it was tried to correlate the hardness of the sample with a new factor, the H_{pm}, instead of the coercivity (classically used for the carbon steel) with successful results

[31]. This new parameter can be descript as half the distance between the position of the two peaks of the relative permeability.
The correlation obtained in this work is not perfect as seen in the previous work but it can be used the same as indicative for the hardness, because they follow more or less the same trend.

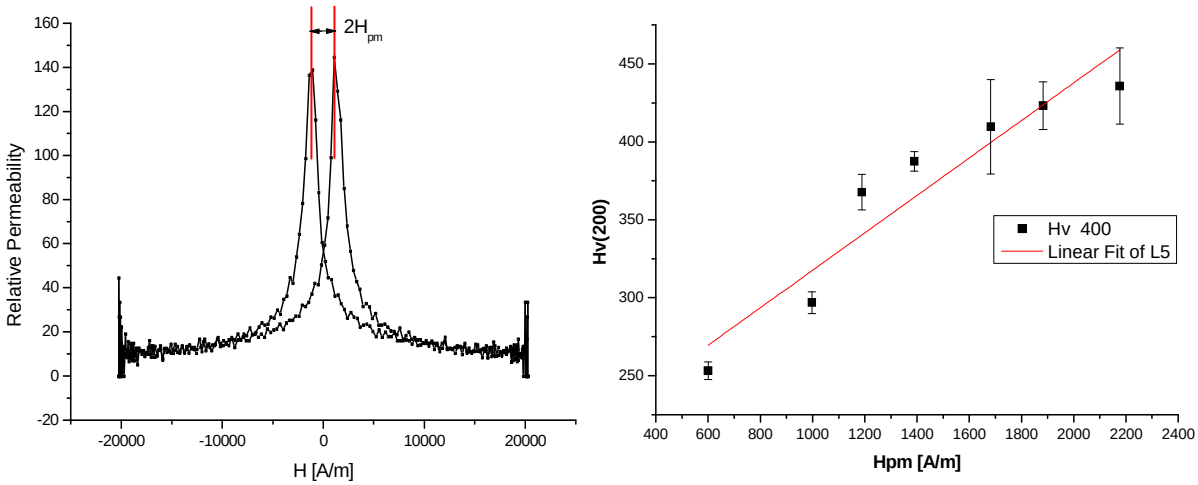

Figure 8: Left, schematic of obtainment of the Hpm. Right, hardness-Hpm correlation.

After 2400s at 900°C is possible to see with OM, with SEM and with Magnetic tests, that a very small amount of ferrite in the samples remains. The magnetic tests, thanks to the high sensibility to the ferromagnetic phases, show that despite the very low quantitative remained, there is a decreasing content of ferrite from the base material (~10% of ferrite remained) to the most deformed sampled (practically disappeared). This means that surely an high grade of cold deformation, therefore an high amount of internal energy, helps the eutectic decomposition of ferrite in secondary austenite and sigma phase, and that leaving the steel more than 40 min in the furnace, all the ferrite could transform in sigma phase and secondary austenite in the most deformed sample. The concept that if the increasing amount of cold rolling accelerate the transformation or simply allows the transformation to begin before respect to the non deformed steel, requires further investigation.
It's quite surprising how a raw measure as the ferrite tester can give, results well approaching the trend of the magnetic tests, it is possible to

see this on the previous graph (orange line), watching the measuring after the treatment at 900°C.

4.9.2 Sigma and austenite analysis

The EBSD analysis was not easy to carry out. The high grade of stress in the material always did't allow to made the test on the 50% and 85% deformed samples, e.g. the Kikuchi lines was very bad with an IQ that was not enough to give a clearly view of the surface phases. The electrolitical etching and the deposition of a very thin layer of gold was tried but the results were again always bad.

Ebsd test, when carried out, confirmed that the formation of the new sigma phase give rise to a state of stress in the neighbor material indeed the IQ map show darker pixel in this areas.

The nucleation of sigma phase clearly starts on the ferrite/austenite boundary, but it precipitates also into the austenite grains drawing some new boundaries. These could be the subgrain borders, where the higher concentration of defects and stacked dislocations (high energy conditions) seems to favor the nucleation of the new brittle phase.

Another interesting result shows, with the increase in deformation, that the ferrite decomposition seems to be more prone to give secondary austenite instead of sigma phase. Theoretically the eutectic decomposition should give 50% of σ and 50% of γ_2 but this is not sure, the percents could be different.

Indeed, it is shown that the content of sigma in the sample rolled at 50% is higher than in the sample rolled at 85%.

The pictures in the EBSD chapter show the phase maps of the samples after the treatment and the following table summarize the results of all the measurements taken.

austenite %	sigma %	
81,13	12,83	BM
70,4	26	50%
88,45	10,5	85%

Table 5 Average contents of austenite and sigma phase in the samples after the last treatment.

Each data is an average of no less than 2 measures. It has to be precised that the magnification is 500x for each measure at 400 and base material, for the 900°C treated the data are from 1500X pictures.
A confirm of the high decomposition of ferrite in sigma phase for the most deformed sample, is given by the Mo content in the sigma and austenite phases. As we know, the classical molybdenum content in the austenite is about 2,6-3 %. Also the sigma phase always shows an high content of Mo. Is possible to see, according to the results, that the molybdenum content, after the treatment at 900°C, increases in the austenite, from the classical value of the base material, to the almost twice of the most deformed. This, while the molybdenum content in the sigma phase, decreases considerably until the deformed at 85% that contain 2.5% less molybdenum. It have again to be précised that the analyzed picture are not at the same magnification, a picture at 500x represents well the material, and it is good for the ebsd in the not deformed material but the things change a lot in the most deformed sample. Here it was possible to take picture at minimum 1500x, this because of the very fine structure that lead to a completely confused picture at 500x, (one of the limits of the EBSD technique). Unfortunately a picture taken at 1500x is less representative of the material because taken at higher magnification. The following table summarizes the results of the chemical analysis.

Mo % content in γ and σ.

	BM	50% th. Red.	85% th. Red.
No treated	3,19	2,84	2,68
Treated at 900C	2,81	3,65	4,27
sigma phase	8,07	7,39	5,42

Table 6: Differences in molybdenum content between samples and treatments, both in austenite both in sigma phase.

Surely so a few measures cannot lead to a conclusion, but further investigation can clarify if this intuition was exact.

Conclusions

The SAF 2507 type superduplex stainless steel was investigated by different magnetic testing methods. The presence of α' martesite after cold rolling was checked in all the samples and the thermally activated decomposition process of the δ-ferrite phase was studied in order to obtain the dependence from the plastic deformation.
Talking about the aim of this work was noticed that:

- The SAF 2507 does not show any α' martensite presence after each rate of plastic deformation. This result is validated by the two different magnetic tests very sensible to any variation of amount of ferromagnetic phase.

- In the samples deformed at 50% and 85%, stripes and bands brighter than the neighbor, was found at the SEM into the austenite grains. No differences in composition were evidenced by EDS analysis.

- After the treatment for 2400s at 400°C it's noticed a partitioning of the ferrite grains in all the samples except those deformed at 65% and 85%. This phenomena was revealed also in a SAF 2205 after a similar treatment.

- The coercivity measured with the forster instrument gives a good correlation with the hardness only for the first two and the final sample. Slightly better is the correlation with the H_{pm} parameter

- The precipitation of sigma phase is enhanced by the plastic deformation, magnetic tests found that in the sample cold rolled at 50%, 65% and 85% the ferrite is almost totally disappeared to give $\sigma+\gamma_2$

- In the OM and SEM analysis was never found the presence of χ phase after both treatment.

- It seems that the eutectic decomposition of ferrite does not give sigma phase and austenite in the same percents, but it depends on the strain rate. This is confirmed also by the decrease in Mo in the sigma phase. Anyway this topic requires further investigations

References

[1] MAZZOLDI NIGRO VOCI, *Fisica Vol II Elettromagnetismo e Onde*. 2nd Ed. 2002.

[2] D.JILES, *Introduction to magnetism and magnetic materials*. 2nd Ed. 1998.

[3] WILLIAM D. CALLISTER JR, *Material science and engineering: an introduction*, 7th Ed. 2007.

[4] GABRIELE DI CAPRIO, *Gli acciai inossidabili*.

[5] THE IRON AND STEEL SOCIETY, *Steel products manual: Stainless steel*, Publication of The iron and steel society, 1999.

[6] G.M.PAOLUCCI, *Lezioni di Metallurgia Vol 2 Tecnologia dei materiali metallici*, 2nd Ed.

[7] GIOVANNI FASSINA, *Effects of cold rolling on austenite to α' - martensite transformation in 2101 lean duplex stainless steel*, Msc work, 2010.

[8] JUHO TALONEN, *Effect of strain induced α martensite transformation on mechanical properties of metastable austenitic stainless steel*, Doctoral dissertation, 2007.

[9] DAVIDE PEGORARO, *Modificazioni microstrutturali prodotte dalla deformazione plastica nell'acciaio duplex 2507*, Bsc work, 2010.

[10] EDDY PICCOLO, *Caratterizzazione Microstrutturale dell'acciaio duplex SAF 2205 deformato a freddo*, Bsc work, 2008.

[11] BELA LEFFLER, *Stainless steels and their properties*, Outokumpu publication.

[12] ALBERTO TIZIANI, FRANCO BONOLLO, *Acciai inossidabili innovativi, Information seminar*, 1998.

[13] BONARDI, D'ERRICO, MAPELLI, *Microstruttura, trattamenti termici e proprietà meccaniche degli acciai inossidabili bifasici*, Politecnico di Milano pubblication.

[14] BASSANI, PASSARETTI, CALLIARI, BRUNELLI, REBUFFI, *EBSD investigation on a 2507 duplex steel*, proc. of duplex 2007 Grado-Italy

[15] JIMENEZ, CARSI,RUANO, *Characterization of a δ/γ duplex stainless steel*, Journal of material science 35 (2000) pp 907-915.

[16] BERECZ, SZABÓ, SAJÓ, MÉSZÁROS, *Measuring of the amount of σ phase in isothermally aged duplex stainless steel.*

[17] TAVARES, PARDAL, GUERREIRO, GOMES, SILVA, *Magnetic detection of sigma phase in duplex stainless steel UNS S31803*, Journal of Magnetism and Magnetic Materials 322 (2010) pp29–33.

[18] NENNO, TAGAYA, OSOMI, NISHIYAMA, *Electron microscope study of sigma phase precipitation in an Iron-Chromium-Nickel Alloy*. 1963 pp222-231

[19] SPEIDEL, *Nitrogen containing austenitic stainless steels*, Mat-wiss. u. Werkstoiftech. 2006, 37, No. 10 pp 875-880.

[20] KIBEY, LIU, JHOHNSON, SEHITOGLU, *Predicting twinning stress in fcc metals: Linking twin-energy pathways to twin nucleation*, Acta Materialia 55 (2007) pp 6843–685.

[21] HATTESTRAND, LARSSON, CHAI, NILSSON, ODQUIST, *Study of decomposition of ferrite in a duplex stainless steel cold worked and aged at 450–500 ◦C.* Materials Science and Engineering A 499 (2009) pp 489–492.

[22] GOMES DE ABREU, SANTANA DE CARVALHO, DE LIMA NETO, PIRES DOS SANTOS, NOGUEIRA FREIRE, DE OLIVEIRA SILVA, SOUTO MARIO TAVARES. *Deformation Induced Martensite in an AISI 301LN Stainless Steel: Characterization and Influence on Pitting Corrosion Resistance*, Materials Research, Vol. 10, No. 4, (2007) pp 359-366.

[23] RODRIGO MAGNABOSCO, *Kinetics of Sigma Phase Formation In a Duplex Stainless Steel*, Materials Research, Vol. 12, No. 3, (2009) pp 321-327.

[24] TAVARES, PARDAL, DE SOUZA, NETO, DA SILVA, *Magnetic phase quantification of the UNS S32750 superduplex stainless steel*, Journal of Alloys and Compounds 416 (2006) pp 179–182.

[25] SHII-HON CHOI, YOUNG-SOOL JIN, *Evaluation of stored energy in cold-rolled steels from EBSD data*, Materials Science and Engineering A 371 (2004) pp 149–159.

[26] STRADOMSKY, DIYA, *Sigma phase precipitation in duplex phase stainless steels*, publication of Czestochowa University of Technology, Institute of Materials Engineering

[27] WEISBRODT-REISCH, BRUMMER, HADLER, WOLBANK, WERNER, *Influence of temperature, cold deformation and a constant mechanical load on the microstructural stability of a nitrogen alloyed duplex stainless steel*. Materials Science and Engineering A 416 (2006) pp 1–10.

[28] DOBRANSZKY, SZABÓ, BERECZ, HROTKO, PORTKO, *Energy-dispersive spectroscopy and electron backscatter diffraction analysis of isothermally aged SAF 2507 type superduplex stainless steel*, Spectrochimica Acta Part B 59 (2004) pp 1781– 1788.

[29] RAVI KUMAR, SAILAJA SHARMA, SAHU, *Effect of thermal cycles on heavily cold deformed AISI 304L austenitic stainless steel*, Materials Science and Engineering A 527 (2010) pp 875–882.

[30] HADJI,BADJI, *Microstructure and Mechanical Properties of Austenitic Stainless Steels After Cold Rolling*, JMEPEG (2002) 11 pp 145-151.

[31] I.MÉSZÁROS, SZABÓ, *Complex magnetic and microstructural investigation of duplex stainless steel*, NDT&E International 38 (2005) pp 517–521.

[32] I.MÉSZÁROS, *Magnetic characterization of duplex stainless steel*, Physica B 372 (2006) pp 181–184.

[33] I.MÉSZÁROS, DÉVÉNYI, HIDASI, POTGIETER, GINSZTLER, *Magnetic investigations of stainless steels*, Int. J. Pres. Ves. & Piping 61 (1995) pp 471-478.

[34] MAITLAN, SITZMAN, *Electron Backscatter Diffraction (EBSD) Technique and Materials Characterization Examples*, Scanning microscopy for nanotechnology techniques and applications (2007) pp 41-75.

[35] GRIFFIN, *A super duplex success story*, Stainless steel world (June 2009) pp 1-5.

[36] MANFRIN, *Effetto della deformazione a freddo sulle trasformazioni di fase per l'acciaio SAF2507 indotte da trattamento termico*, Msc work, 2011.

[37] CANIGLIA, Precipitazione *di fasi secondarie negli acciai duplex*, Msc work, 2000.

[38] www.mse.iastate.edu

[39] www.scuolaelettrica.it

[40] www.magneticmicrosphere.com

[41] www.stainless-steel-tube.org

[42] www.msm.cam.ac.uk

[43] www.ebsd.com

[44] www.sdm.buffalo.edu

[45] www.helmut-fischer.com

[46] www.azobuild.com